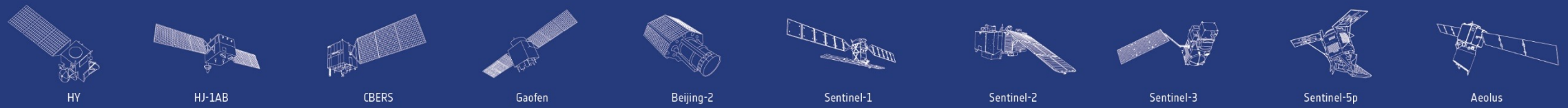

2023 DRAGON 5 SYMPOSIUM

3rd YEAR RESULTS REPORTING

11-15 SEPTEMBER 2023

[PROJECT ID. 59257]

[MAPPING FOREST PARAMETERS AND FOREST DAMAGE FOR SUSTAINABLE FOREST MANAGEMENT FROM DATA FUSION OF SATELLITE DATA]

Dragon 5 3rd Year Results Project

<14/SEPT/2023, 9:00AM - 10:30AM CEST>

ID. 59257

PROJECT TITLE: MAPPING FOREST PARAMETERS AND FOREST DAMAGE FOR SUSTAINABLE FOREST MANAGEMENT FROM DATA FUSION OF SATELLITE DATA

PRINCIPAL INVESTIGATORS: Prof. Xiaoli Zhang and Dr. Langning Huo

CO-AUTHORS: Ning Zhang, Henrik Persson, Yueting Wang, Eva Lindberg, Niwen Li, Ivan Huuva, Guoqi Chai, Lingting Lei, Long Chen, Xiang Jia, Zongqi Yao

PRESENTED BY: Langning Huo

Beijing Forestry University

Swedish University of Agricultural Sciences

Project Introduction

Background:

- This project concerns the topic Ecosystems and spans the subtopics Collaborative estimation of forest quality parameters and Forest and grassland disaster monitoring.

Objective:

- Study and explore remote sensing techniques in forest applications, especially on data fusion of satellite images, laser scanning, and hyperspectral drone images.

The research contents:

- Tree species classification
- Forest parameter estimation
- Forest insect damage detection

EO Data Delivery

ESA Third Party Missions	No. Scenes
1. Sentinel-1	173
2. Sentinel-2	380
3. SPOT	2
4. Radarsat-2	1
5. WorldView-3 SWIR	1
6.	
Total:	555

Study areas:

- Gaofeng, Weihai, Fushun, Lu'an, Wangyedian, Genhe and Pu'er in China
- Remningstorp in Sweden

Chinese EO data	No. Scenes
1. Gaofen-1	55
2. Gaofen-2	110
3. Gaofen-6	150
4.	
5.	
6.	
Total:	315

Study areas:

- Gaofeng, Weihai, Fushun, Lu'an, Wangyedian, Genhe and Pu'er in China

Study area in China

- Field investigation of forest parameters was conducted in **Gaofeng and Genhe**. The inventory recorded diameter at breast height, tree height, under branch height, and the coordinates of the plots.
- Spectral information was collected from healthy and pine nematode-infested forests at different stages in the **Fushun and Lu'an** study areas.
- The information of tree species, forest changes and disturbance in **Pu'er** was collected. And the occurrence status and geographical distribution information of Simao pine bark beetle diseases were recorded.

Study area in Sweden

- Southern Sweden
- 1,200 ha productive forest
- Active forest management
- Reference data for RS
- Bark beetle outbreaks in 2018

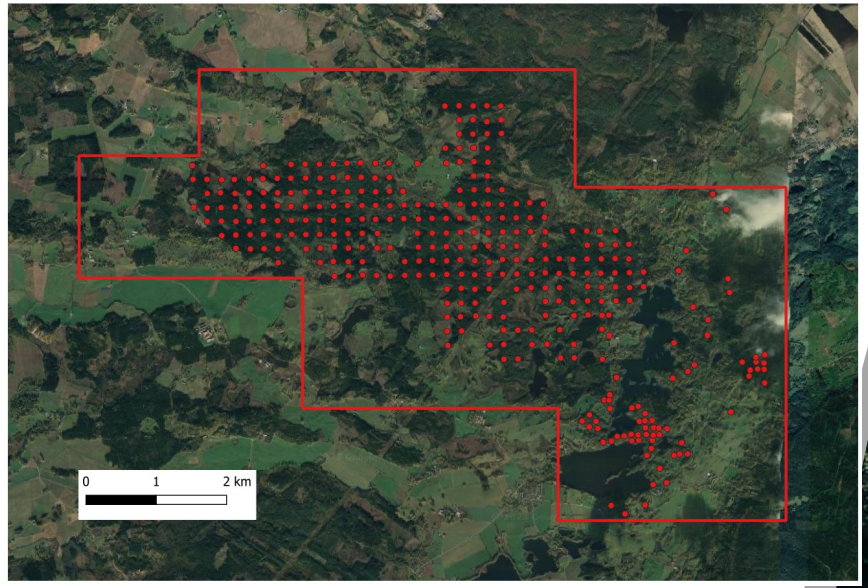

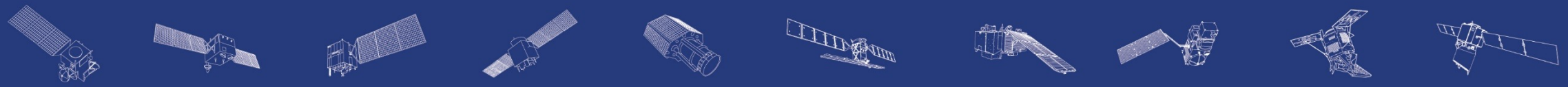

Tree Species Classification

Beijing Forestry University

Tree Species Classification

Tree Species Classification by few-shot learning (Stand scale)

- Propose an improved prototypical networks (**IPrNet**) , a **CBAM-P-Net** model of the prototype network combined with an attention mechanism, and a **Proto-MaxUp+CBAM-P-Net** model of the CBAM-P-Net combined with a data enhancement strategy
- Use UAVs hyperspectral data
- Obtain good classification results for **8 major tree species** in southern China

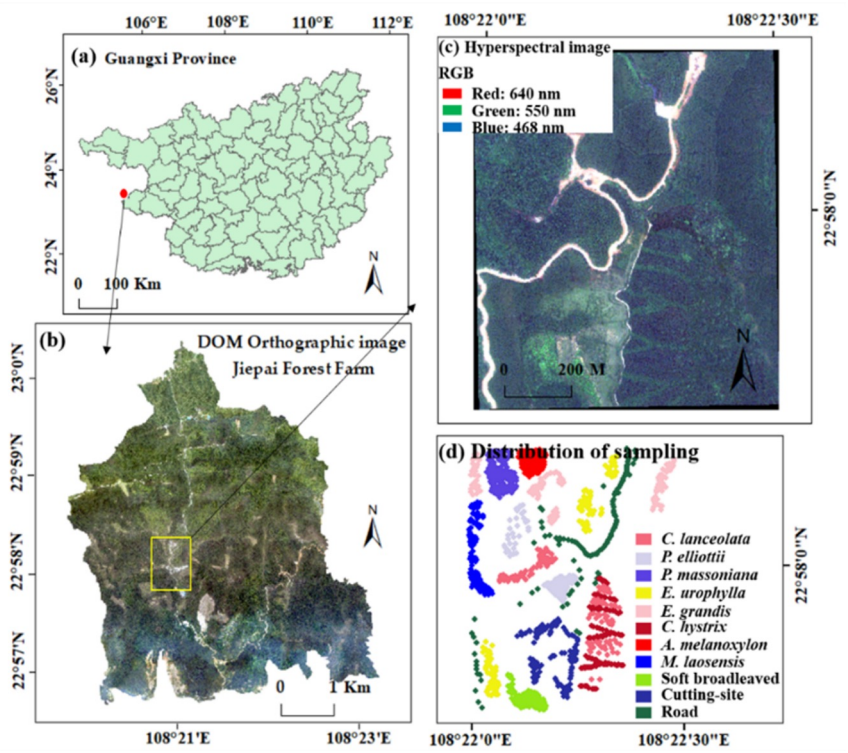

Categories	Samples	
	Trian	Test
Cunninghamia lanceolata	96	24
Pinus massoniana	96	24
Pinus elliottii	96	24
Eucalyptus grandis	96	24
Eucalyptus urophylla	96	24
Castanopsis hystrix.	96	24
Mytilaria laosensis	96	24
Acacia melanoxylon	96	24
Other broadleaf forest	96	24
Road	96	24
Cutting-site	96	24
Total	1056	264

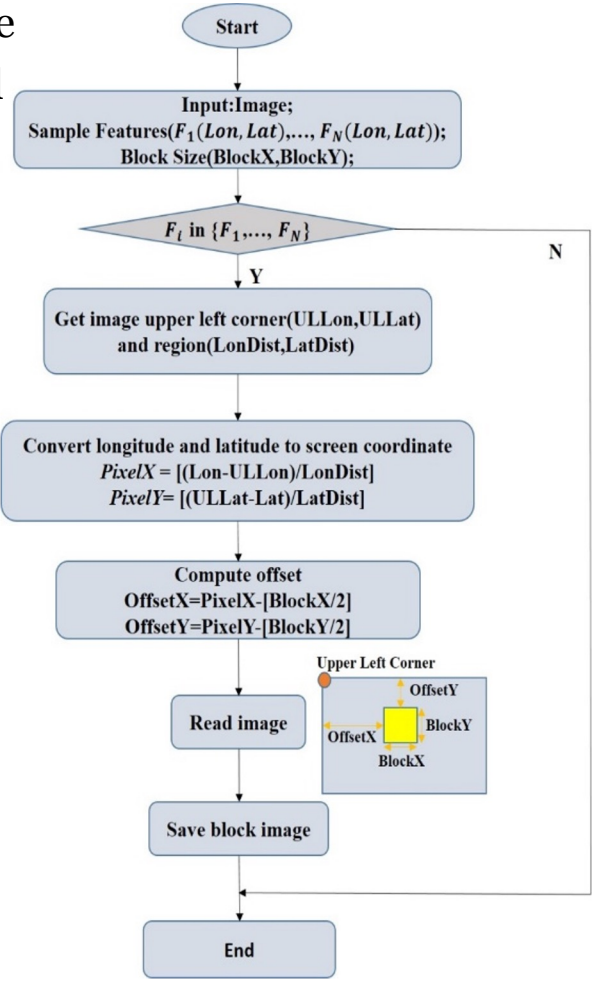

Tree Species Classification

IPrNet Classification Framework

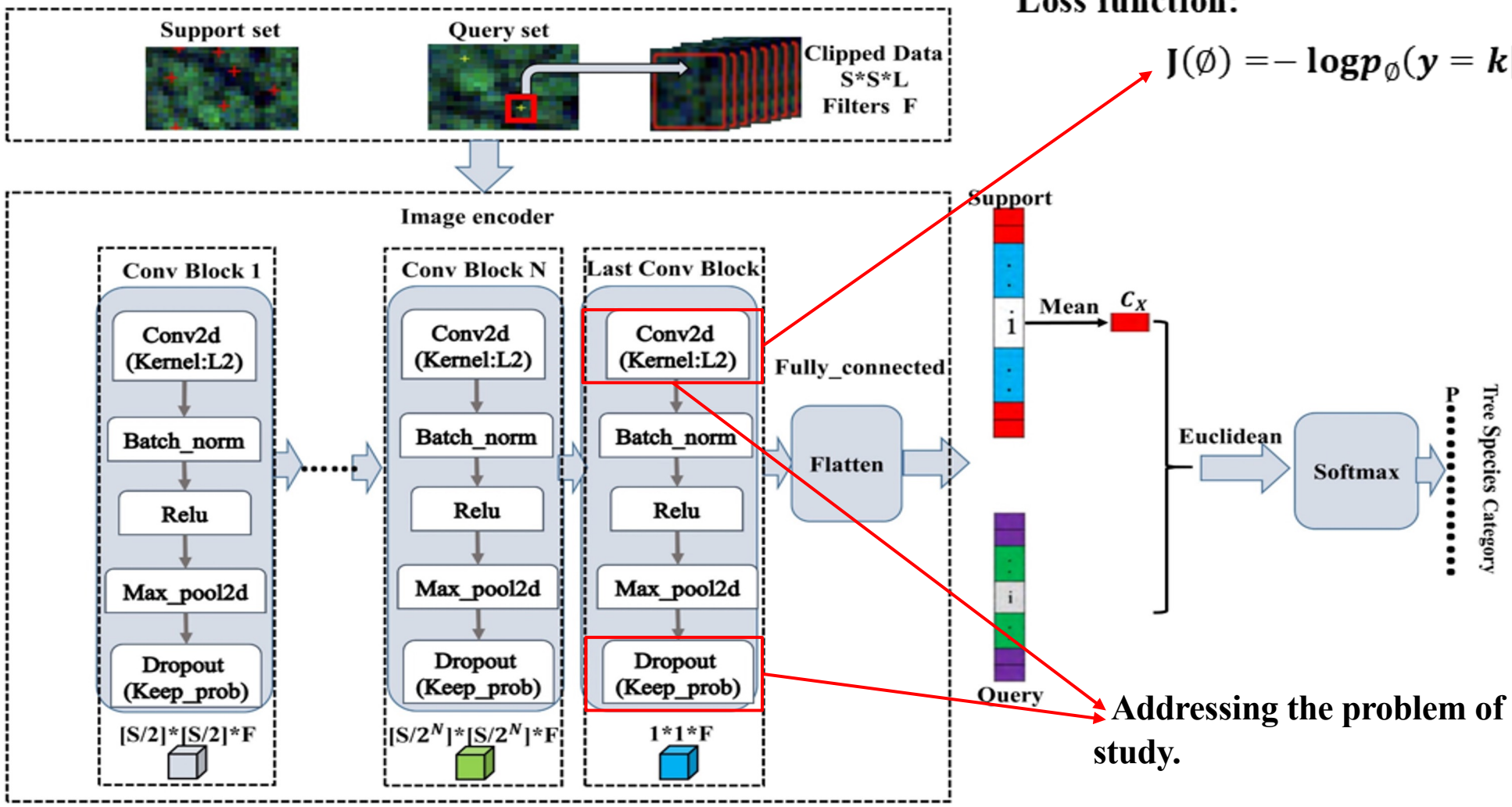

Loss function:

$$J(\emptyset) = -\log p_{\emptyset}(y = k|x) + \alpha_2 \sum_{w} w^2$$

Addressing the problem of overfitting in this study.

Tree Species Classification

CBAM-P-Net Classification Framework

Target:

Improving the feature extraction efficiency
Overcoming the dimensional dilemma

CBAM Combination Strategy:

- **Channel attention is applied globally**
- **Spatial attention is applied locally**
- **Channel First → Global first and then local**

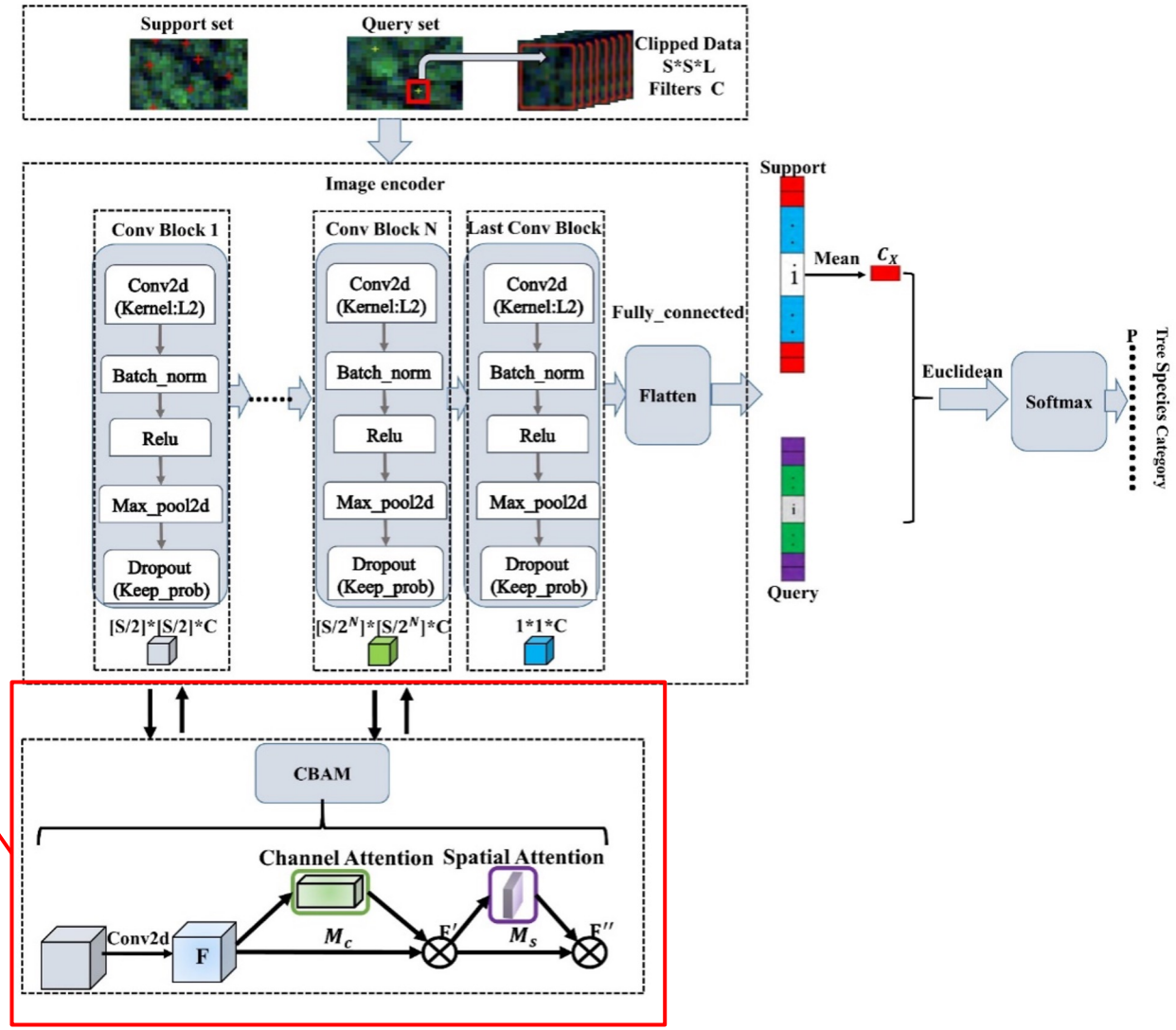

Tree Species Classification

Proto-MaxUp Classification Framework

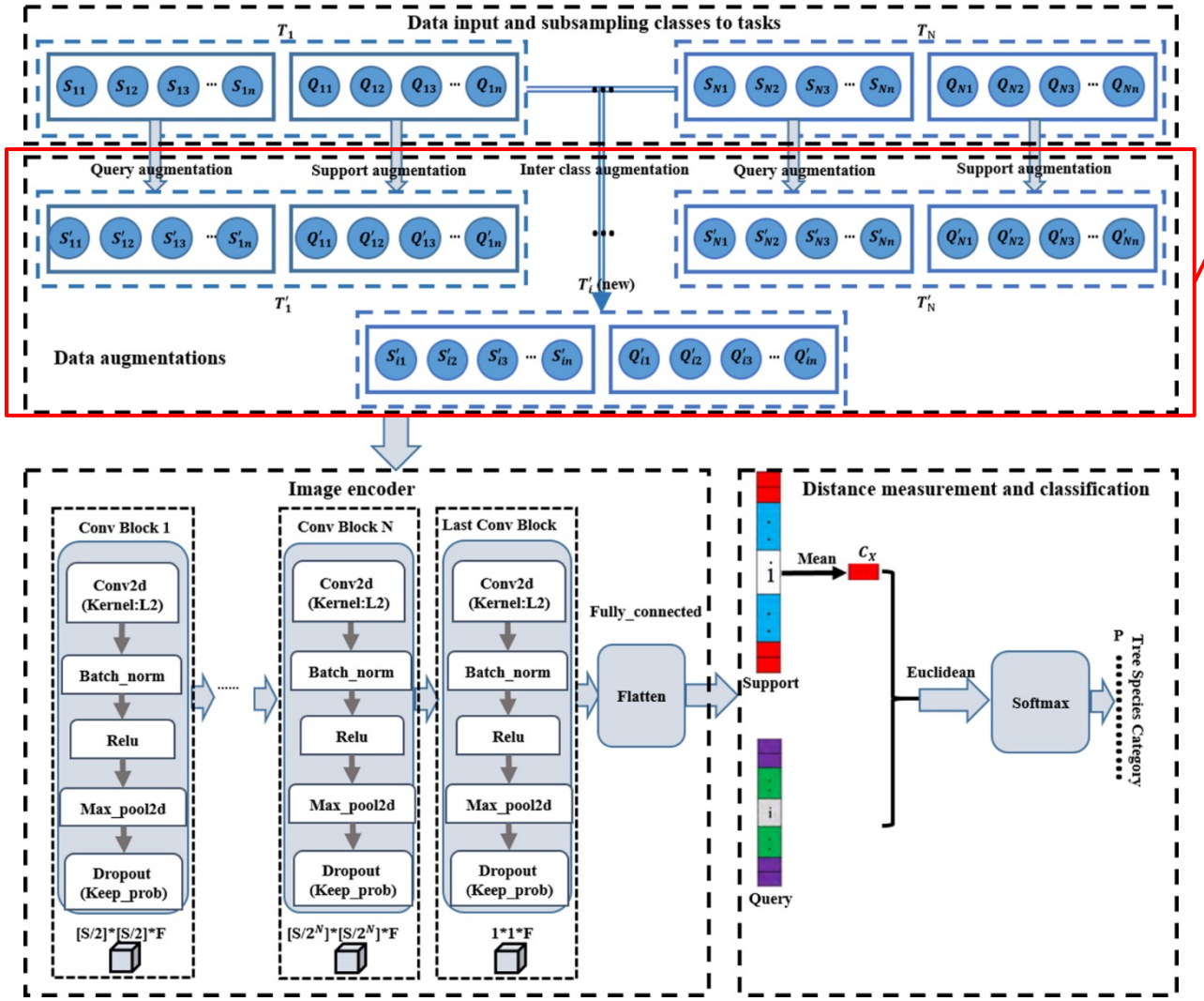

Data augmentation:
- **Improving sample diversity.**
- **Minimizing the overfitting problem.**

Proto-MaxUp:
- **Adversarial training: minimize the maximum loss**
- **Solving the issue of saddle-point**

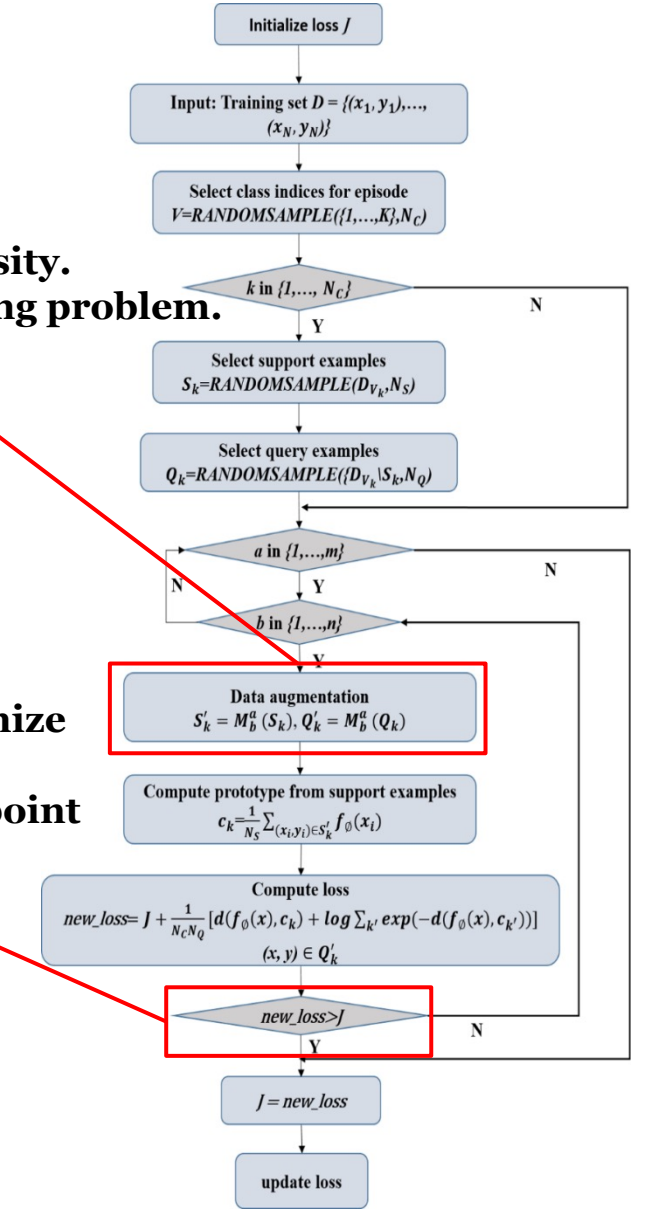

Tree Species Classification

SCL-P-Net Classification Framework

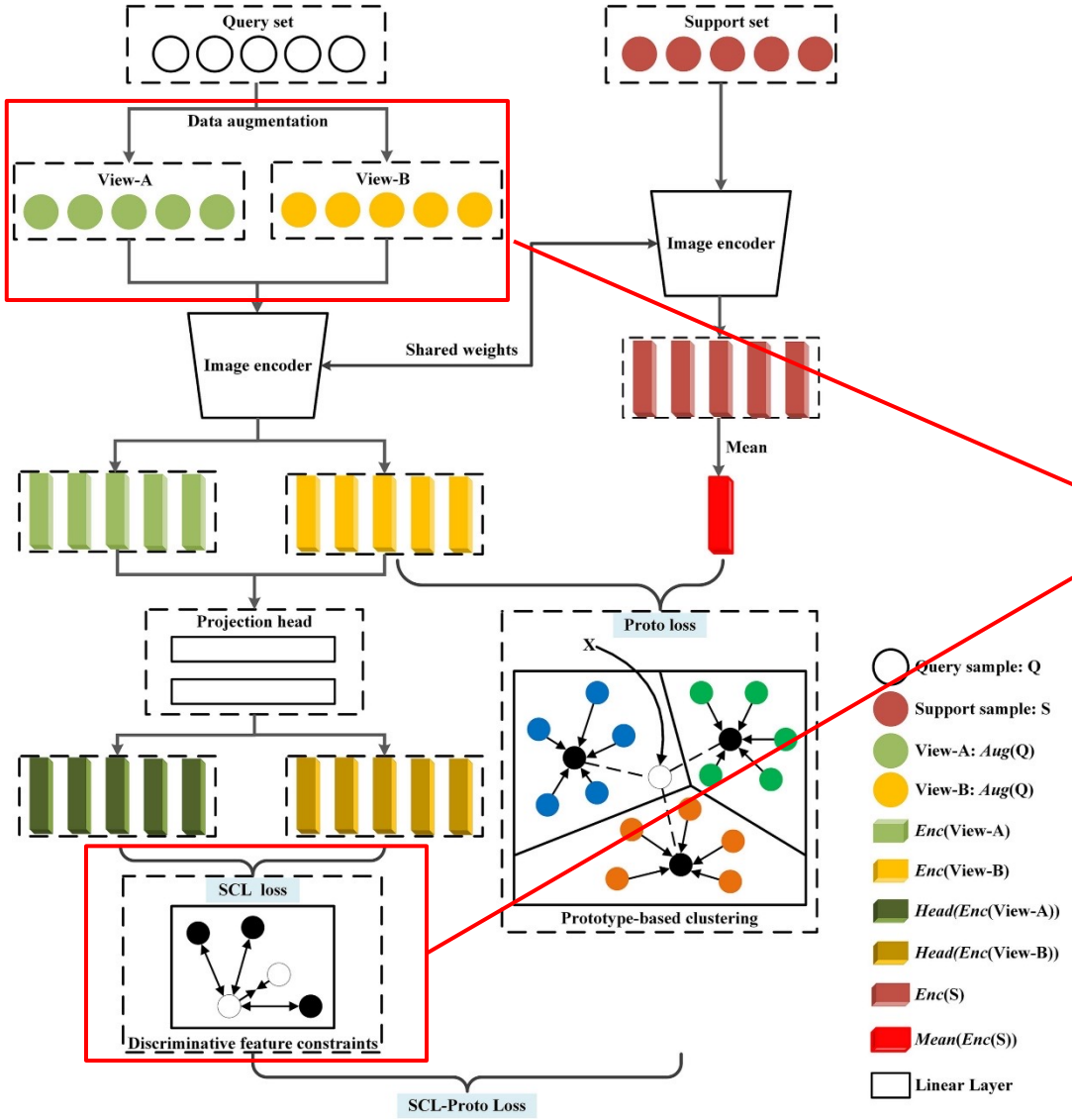

Supervised Contrastive Learning for combination of data augmentation and feature enhancement Algorithms:

- Enriching sample diversity.

- In the feature space, positive (same class) samples are clustered and negative (different class) samples are separated.

Tree Species Classification

SCL-P-Net Classification Map

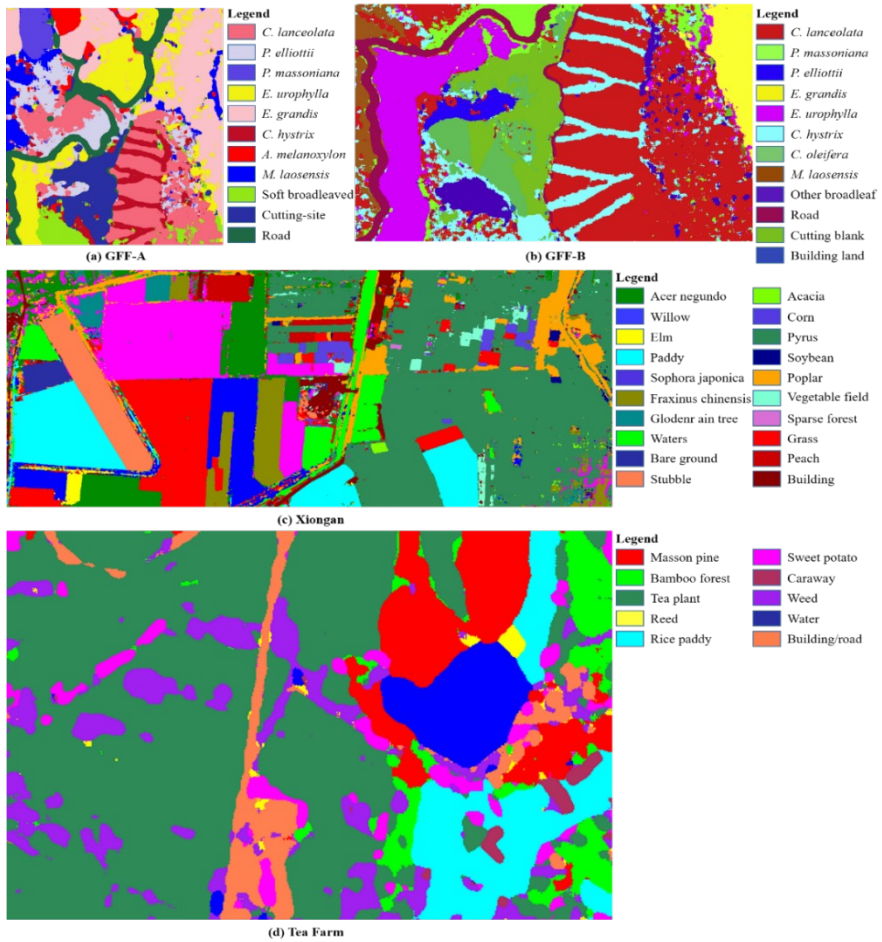

Classification maps of SCL-P-Net with different datasets

Dataset	GFF-A	GFF-B	Xiongan	Tea Farm
OA (%)	**99.23**	**98.39**	**99.30**	**99.54**
WOA (%)	99.23	98.41	99.26	99.87
AA (%)	99.24	98.78	97.54	99.32
Class A (%)	96.91	97.93	99.18	99.72
Class B (%)	98.95	98.14	99.70	97.86
Class C (%)	100.00	97.36	97.99	99.50
Class D (%)	100.00	99.95	99.93	98.60
Class E (%)	100.00	99.70	99.60	99.88
Class F (%)	96.88	95.44	99.89	99.60
Class G (%)	100.00	99.35	99.96	99.30
Class H (%)	98.88	99.98	99.79	98.87
Class I (%)	100.00	99.67	99.53	100.00
Class J (%)	100.00	97.81	99.96	99.89
Class K (%)	100.00	99.99	97.29	-
Class L (%)		100.00	97.46	-
Class M (%)		-	99.36	-
Class N (%)		-	92.24	-
Class O (%)		-	94.92	-
Class P (%)		-	92.05	-
Class Q (%)		-	85.80	-
Class R (%)		-	99.46	-
Class S (%)		-	98.24	-
Class T (%)		-	98.39	-

Chen L., Wu J., Xie Y., Chen E., Zhang X. Discriminative Feature Constraints via Supervised Contrastive Learning for Few-Shot Forest Tree Species Classification Using Airborne Hyperspectral Images, Remote Sensing of Environment, 2023

Tree Species Classification by Deep Learning

- **Improving the feature extraction efficiency**
- **Data augmentation**
- **Feature enhancement**

1. Chen L, Wu J, Xie Y, et al. Discriminative feature constraints via supervised contrastive learning for few-shot forest tree species classification using airborne hyperspectral images[J]. ***Remote Sensing of Environment***, 2023, 295: 113710.
2. Chen L, Wei Y, Yao Z, et al. Data augmentation in prototypical networks for forest tree species classification using airborne hyperspectral images[J]. ***IEEE Transactions on Geoscience and Remote Sensing***, 2022, 60: 1-16.
3. Li Y, Chai G, Wang Y, et al. Ace r-cnn: An attention complementary and edge detection-based instance segmentation algorithm for individual tree species identification using uav rgb images and lidar data[J]. ***Remote Sensing***, 2022, 14(13): 3035.
4. Chen L, Tian X, et al. A New CBAM-P-Net Model for Few-Shot Forest Species Classification Using Airborne Hyperspectral Images[J]. ***Remote Sensing***, 2021, 13, 1269.

Tree Species Classification

Individual-Tree Species Identification by ACE R-CNN

- Propose an attention mechanism, **edge detection** and region-based instance segmentation algorithm (ACE R-CNN)
- Use **UAV LiDAR and RGB** images.
- Obtain good classification results for **6 major tree species** in southern China.

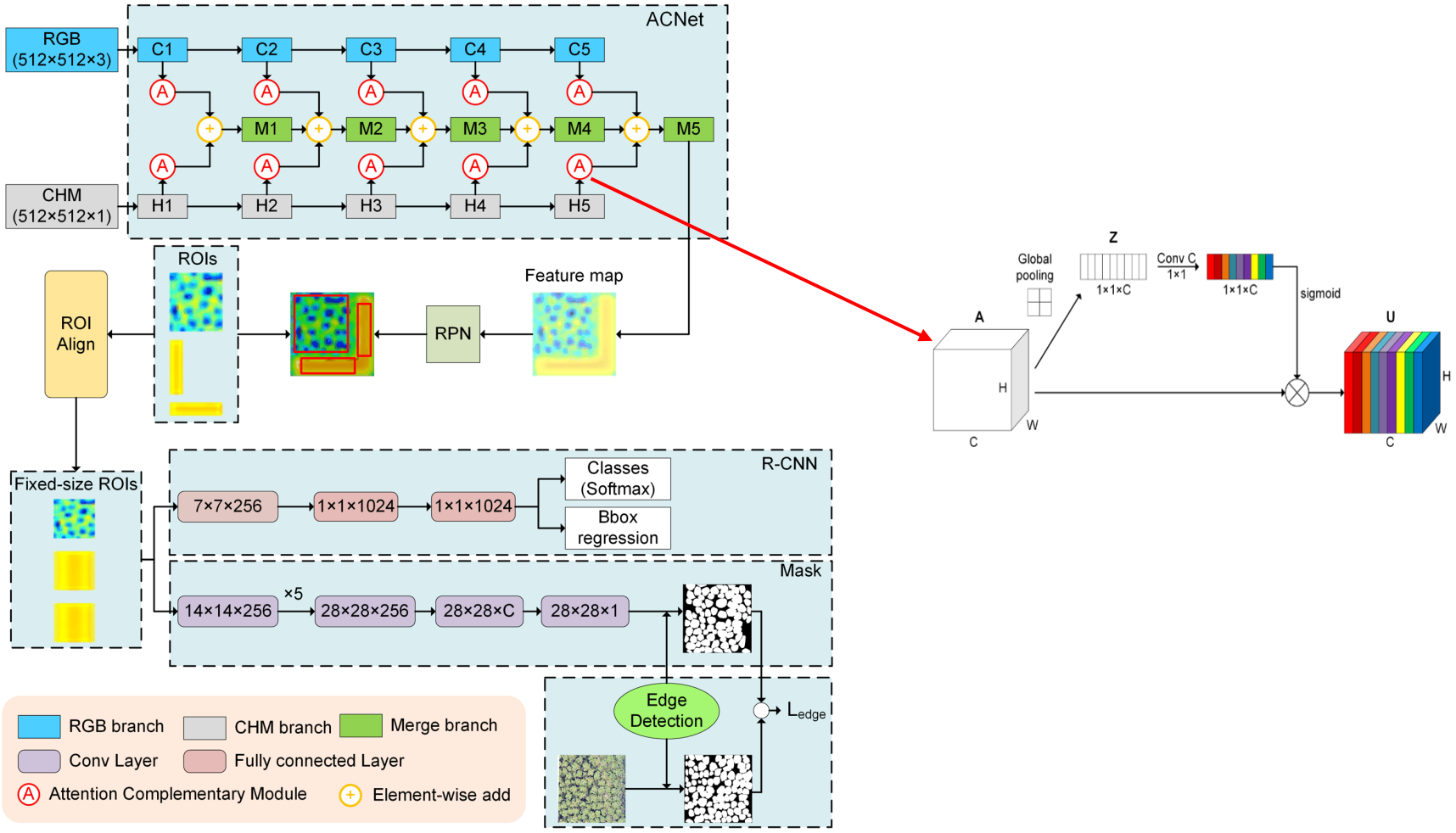

ACE R-CNN Framework

Tree Species Classification

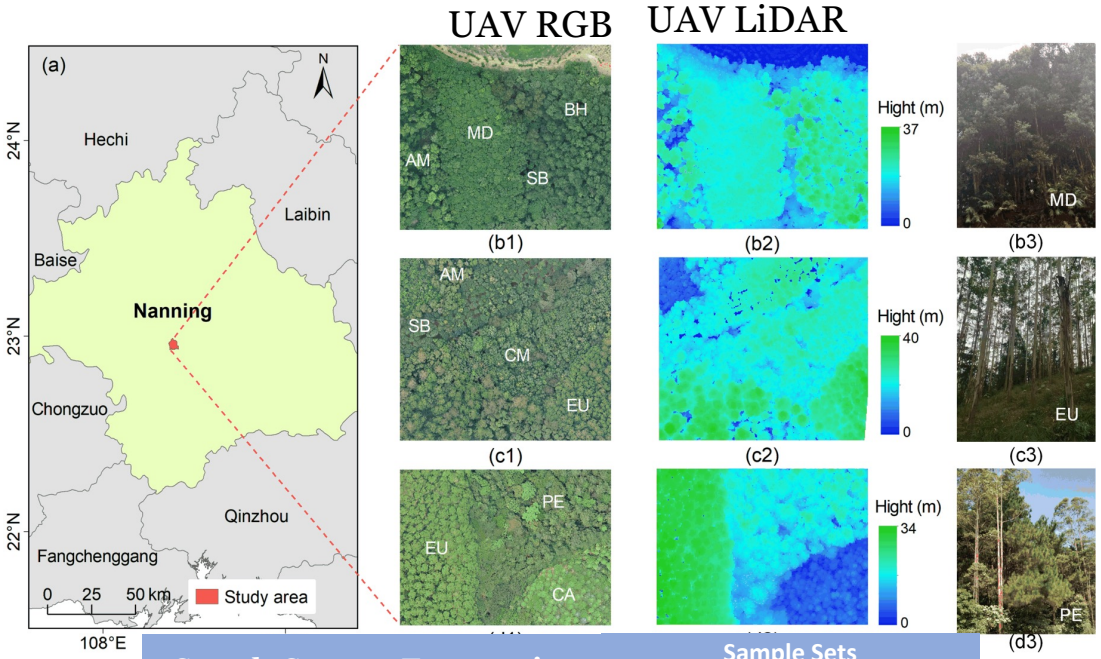

Sample Sets	Tree species	Sample Sets	
		Training Set	Test Set
Experiment area 1	BH	240	172
	MD	291	209
	AM	141	106
	SB	99	80
	Total	771	567
Experiment area 2	AM	146	114
	EU	288	212
	CM	271	192
	SB	235	174
	Total	940	692
Experiment area 3	EU	181	135
	PE	160	116
	CA	147	117
	Total	488	368

Individual-Tree Species Identification Map

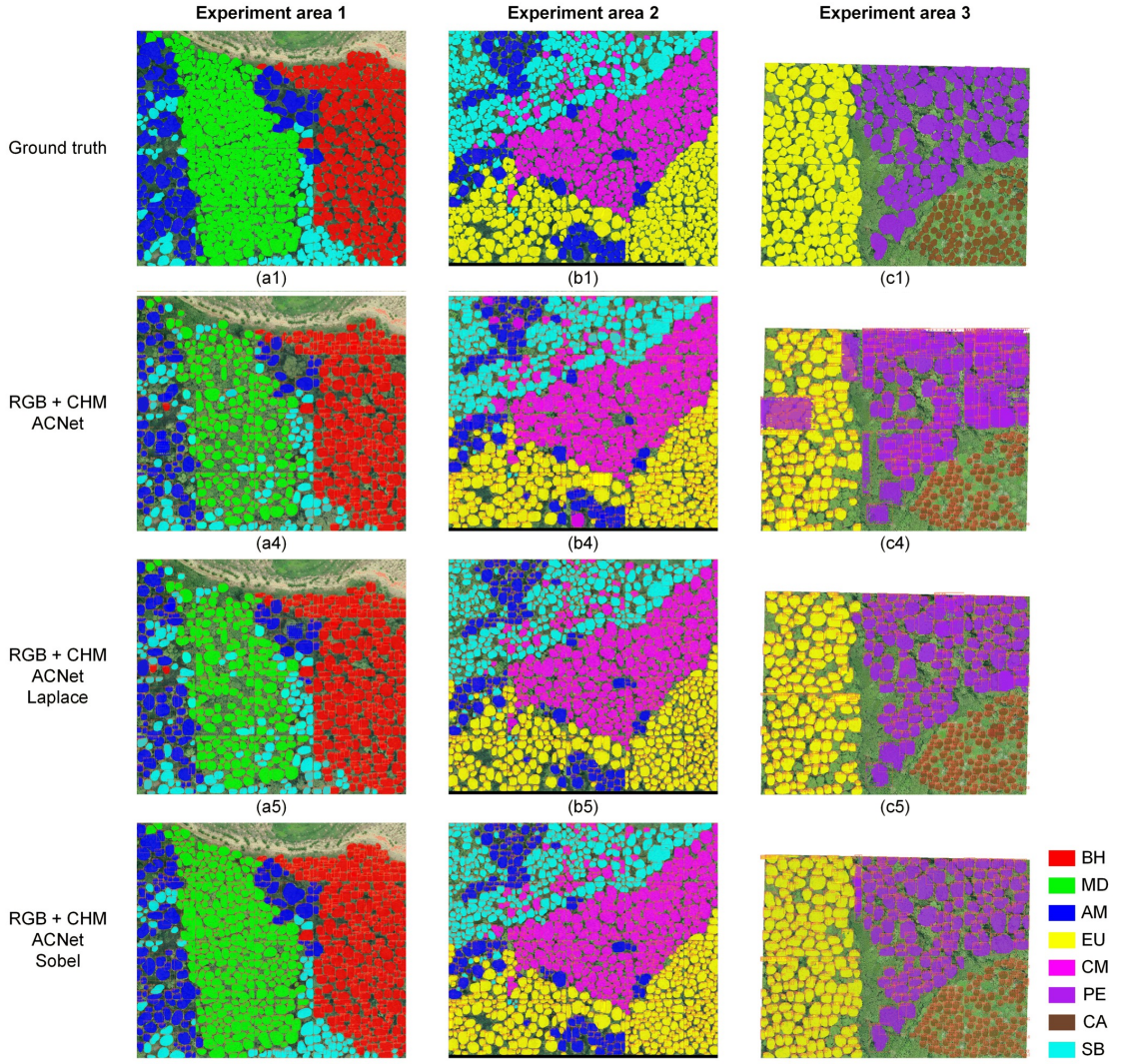

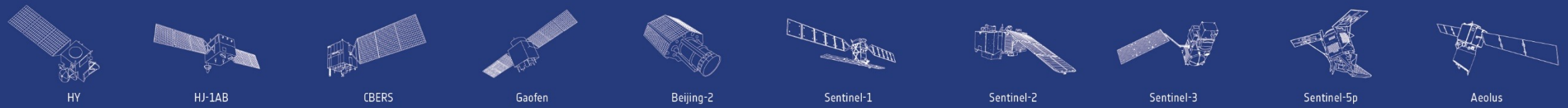

Forest Parameter Estimation

Beijing Forestry University

Forest parameter estimation

Individual tree crowns segmentation using UAV oblique photos

- Field data
- UAV oblique photos
- LiDAR data

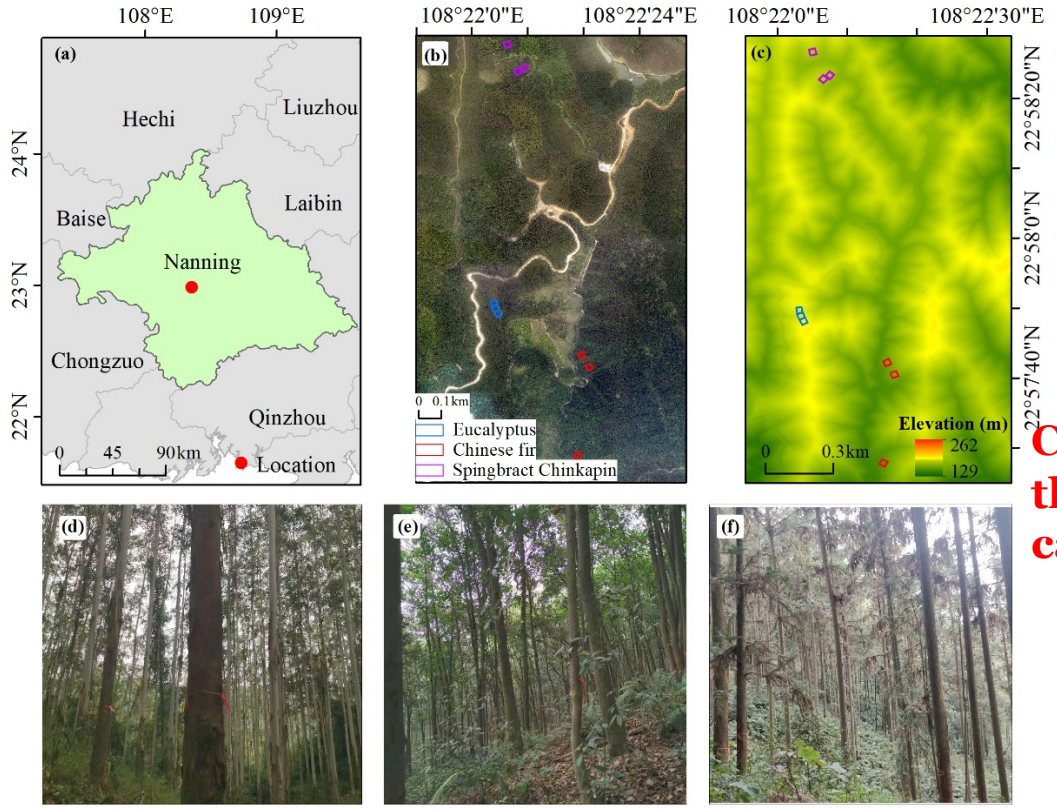

Considering three-dimensional canopy attributes

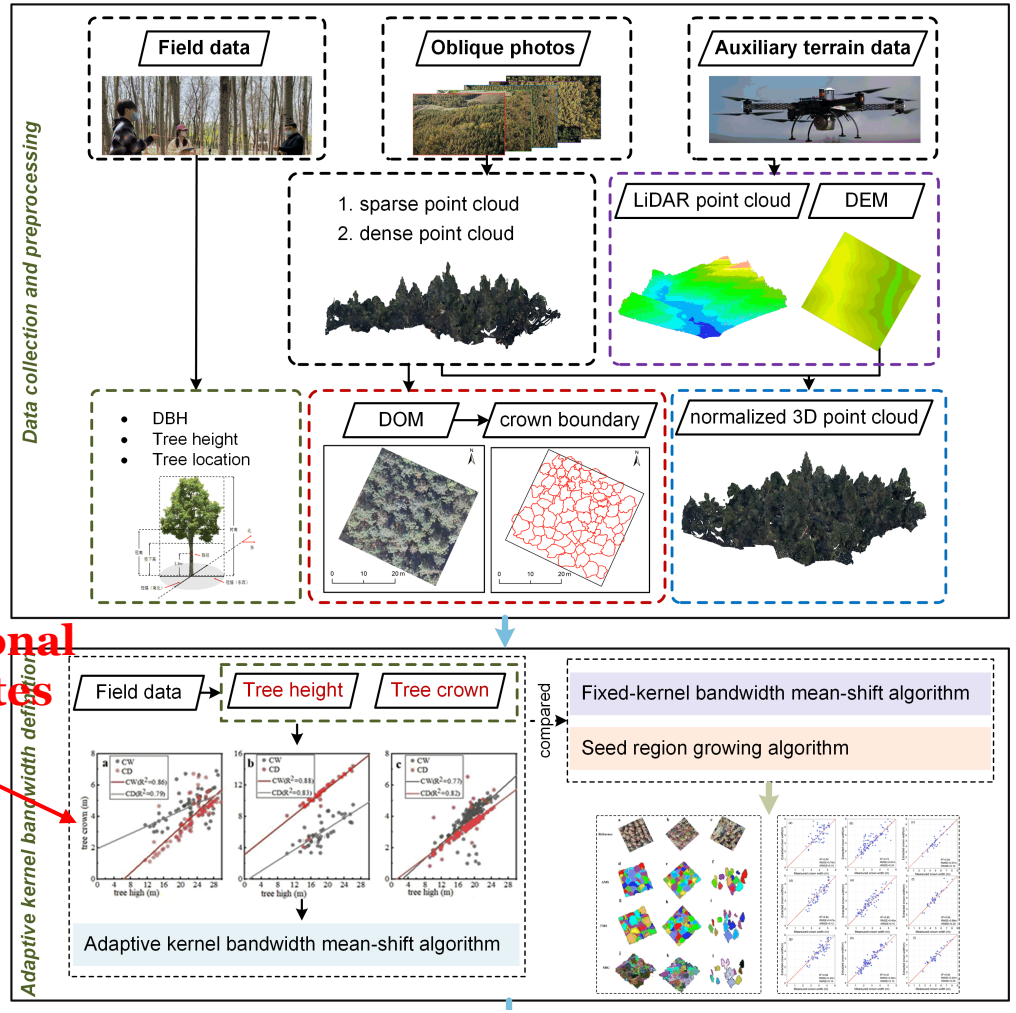

Lei, L.; Yin, T.; Chai, G.; Li, Y.; Wang, Y.; Jia, X.; Zhang, X. A novel algorithm of individual tree crowns segmentation considering three-dimensional canopy attributes using UAV oblique photos. International Journal of Applied Earth Observation and Geoinformation 2022, 112, doi:10.1016/j.jag.2022.102893.

RESEARCH APPROACH

Individual tree crowns segmentation using UAV oblique photos

$$M_{h^s,h^c}(X_B)=\frac{\sum_{i=1}^{n}X_i\,g^s\left(\left\|\frac{X_B^s-X_i^s}{h^s}\right\|^2\right)g^c\left(\left\|\frac{X_B^c-X_i^c}{h^c}\right\|^2\right)}{\sum_{i=1}^{n}g^s\left(\left\|\frac{X_B^s-X_i^s}{h^s}\right\|^2\right)g^c\left(\left\|\frac{X_B^c-X_i^c}{h^c}\right\|^2\right)}-X_B$$

Vector of mean shift at any point

Move towards the maximum of height and density

Kernel function: characterising the contribution of the offset to the mean shift vector

$$g^s\left(\left\|\frac{X_B^s-X_i^s}{h^s}\right\|^2\right)=\begin{cases}\exp\left(-\frac{1}{2}\left\|\frac{X_B^s-X_i^s}{h^s}\right\|^2\right) & if\ \left\|\frac{X_B^s-X_i^s}{h^s}\right\|^2\le 1\\ 0 & otherwise\end{cases}$$

horizontal kernel function

Move towards the maximum of density

Horizontal kernel bandwidth

$$g^c\left(\left\|\frac{X_B^c-X_i^c}{h^c}\right\|^2\right)=\begin{cases}1-\left\|1-dist(X_B^c,X_i^c)\right\|^2 & if\ mask(X_B^c,X_i^c)=1\\ 0 & otherwise\end{cases}$$

vertical kernel function

Move towards the maximum of height

vertical kernel bandwidth

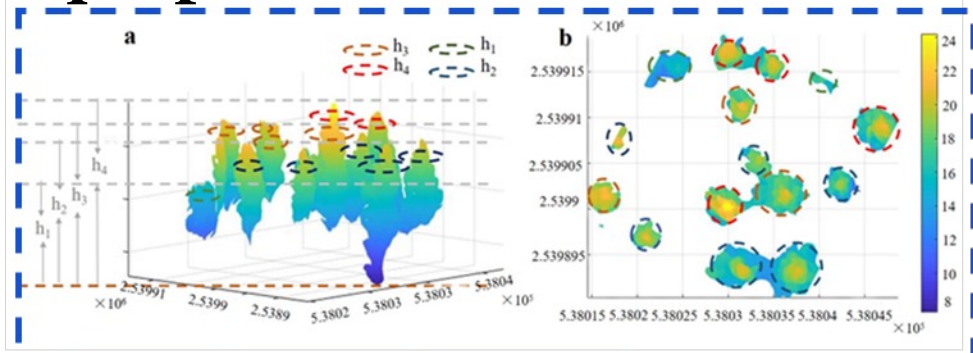

Species	Horizontal	Vertical
Eucalyptus	$h^s(X_i)=0.16\times z_i$	$h^c(X_i)=0.26\times z_i$
Spingbract Chinkapin	$h^s(X_i)=0.2\times z_i$	$h^c(X_i)=0.25\times z_i$
Chinese fir	$h^s(X_i)=0.3\times z_i$	$h^c(X_i)=0.4\times z_i$

tree height

crown length and crown width

Adaptive kernel bandwidth

Fixed kernel bandwidth

$$mask(X_B^c,X_i^c)=\begin{cases}1 & if\ X_B^c-\frac{h^c}{4}\le X_i^c\le X_B^c+\frac{h^c}{2}\\ 0 & otherwise\end{cases}$$

$$dist(X_B^c,X_i^c)=\begin{cases}\min\left\{\left\|\frac{(X_B^c-\frac{h^c}{4})-X_i^c}{\frac{3h^c}{8}}\right\|,\left\|\frac{(X_B^c+\frac{h^c}{2})-X_i^c}{\frac{3h^c}{8}}\right\|\right\} & if\ mask(X_B^c,X_i^c)=1\\ 0 & otherwise\end{cases}$$

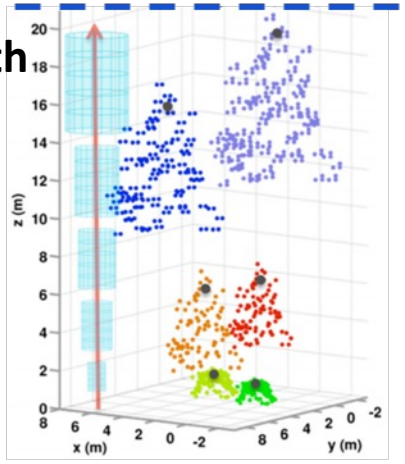

Forest parameter estimation

Individual tree crowns segmentation using UAV oblique photos

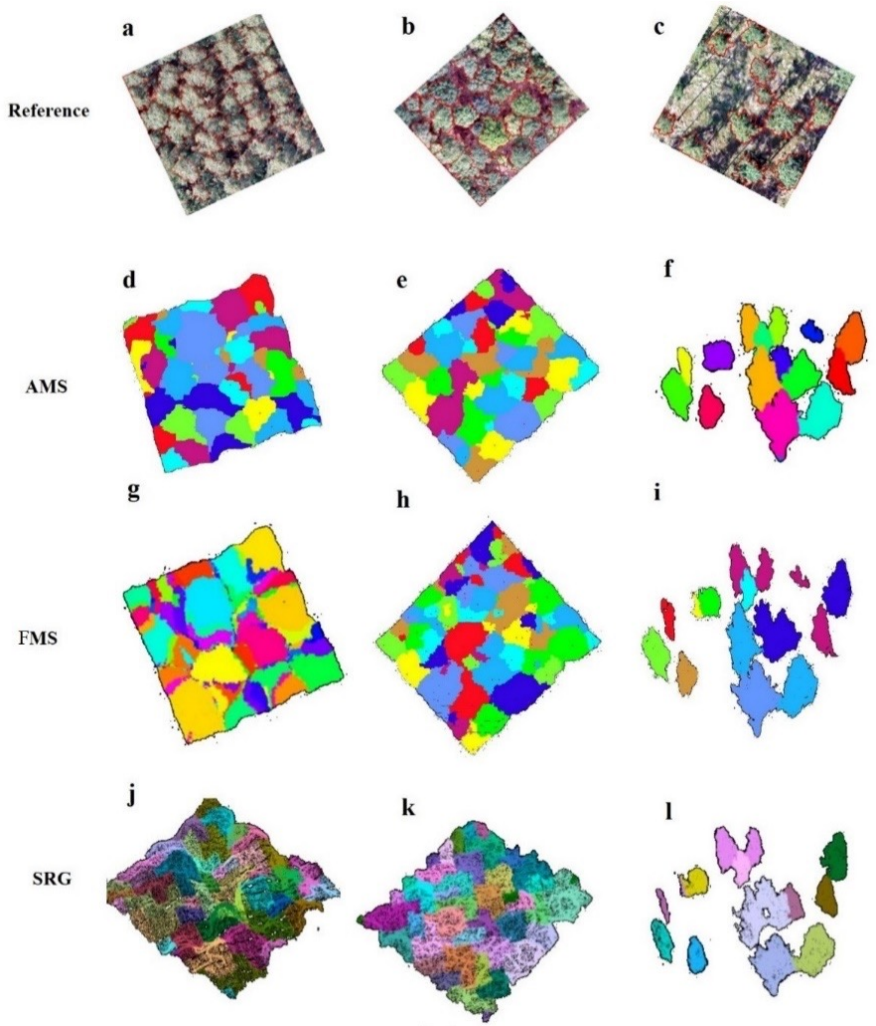

The results of ITCs segmentation (a, d, g, j are Eucalypts, b, e, h, k are Spingbract Chinkapin and c, f, i, l are Chinese fir.)

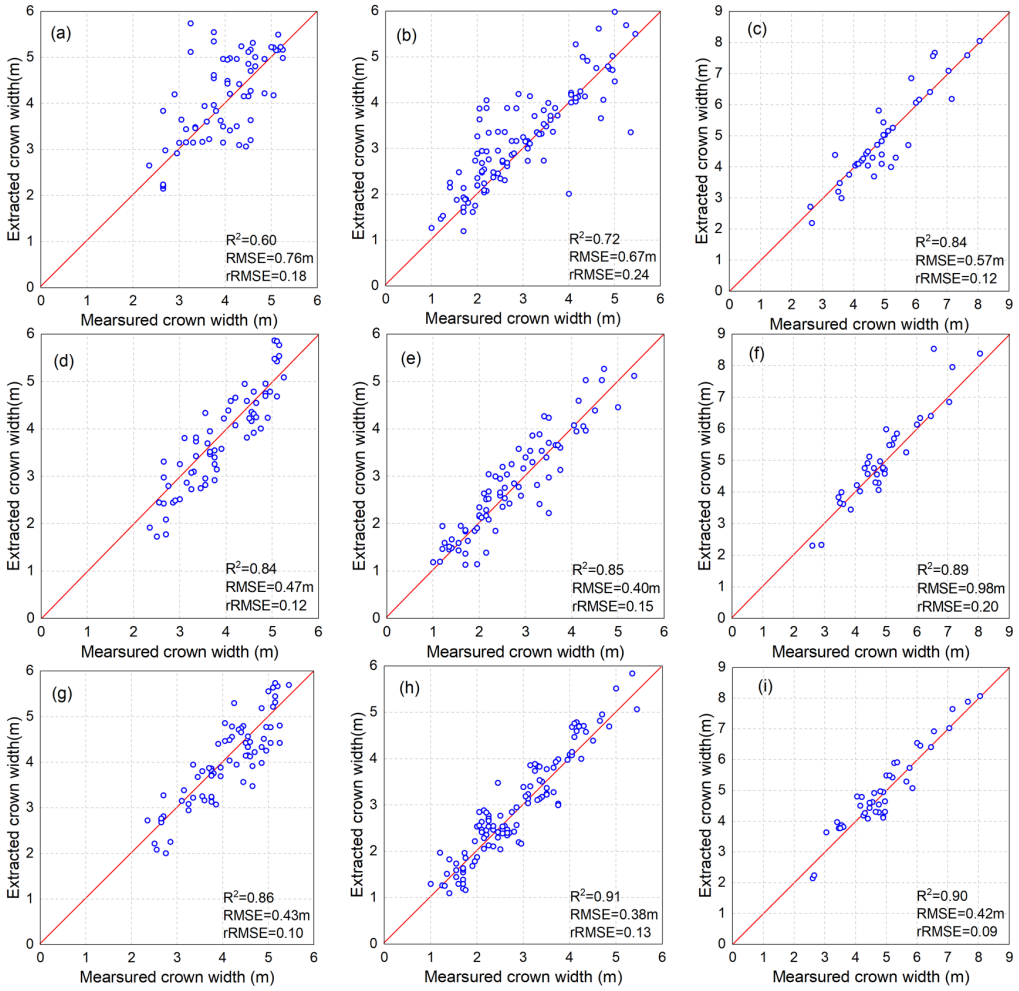

The scatter plots of measured crown width and extracted crown width obtained by the three different methods

- Flexible setting of kernel bandwidth to segment ITC for each tree based on tree height.
- High accuracy can be achieved in both tree top detection and canopy width extraction.
- Appropriate reduction of point cloud density can balance efficiency and accuracy.
- The application of AMS algorithm in LiDAR data is still possible.

Individual Tree above-ground biomass estimation using UAV oblique photos

Type	Variable	Formula	Describe
RGB space	Max_i	——	Maximum intensity
	Min_i	——	Minimum intensity
	$Mean_i$	——	Mean intensity
	sum_i	$sum_i = \sum_{i=1}^{n}(0.2\times R_i + 0.72\times G_i + 0.07\times B_i)$	Total intensity
	sum_{sqrt_i}	$sum_{sqrt\_i} = \sqrt{sum_i}$	Square root of intensity value
HSI space	I_{MAX}	——	Maximum intensity
	I_{MIN}	——	Minimum intensity
	I_{MEAN}		
	I_{SUM}		
	I_{SUM_SQRT}		
Hight variables	H_{mad}		
	H_{AIQ}		
	$H_{kurtosis}$	H_{kurt}	
	H_{cv}		
	H_{ratio}		
	H_{stddev}	H_{stddev}	
	$H_{variance}$	$H_{variance} = \frac{\sum_{i=1}^{n}(Zi-\overline{Z})^2}{n}$	Variance of Z values of all points in a statistical unit
	$H_{skewness}$	$H_{skewness} = \frac{\frac{1}{n}\sum_{i=1}^{n}(Zi-\overline{Z})^3}{(\frac{1}{n-1}\sum_{i=1}^{n}(Zi-\overline{Z})^2)^{\frac{3}{2}}}$	Height skewness
	$H_{1\ldots 99th}$	——	1… 99% cumulative height percentile
	$H_{max,\ min,\ mean,\ median}$	——	The maximum, minimum, average and median of the point cloud after normalization
	$P_{1st,\ldots,99th}$	——	75%, 95% high percentile
density variables	$D_{0,\ldots,9}$	——	The proportion of height points greater than 30%, 50%, 70%, and 90% to all points
Vegetation index	$CIVE$	$CIVE = 0.44R - 0.88G + 0.398 + 18.79$	Color index of vegetation [53]
	ExG	$ExG = 2G - R - B$	Excess green index [54]
	$ExGR$	$ExGR = ExG - 1.4R - G$	Excess green minus excess red index [55]
	GLA	$GLA = \frac{2\times G-R}{2\times G+R+B}$	Green leaf algorithm [56]
	$NGRDI$	$NGRDI = \frac{G-R}{G+R}$	Normalized green–red difference index [56]
	VEG	$VEG = \frac{G}{R^a B^{(1-a)}}, a = 0.67$	Vegetation index [57]
	COM	$COM = 0.25ExG + 0.3ExGR + 0.33CIVE + 0.12VEG$	Combination index [58]

Feature variables

- RGB space
- HSI space
- Hight variables
- density variables
- Vegetation index

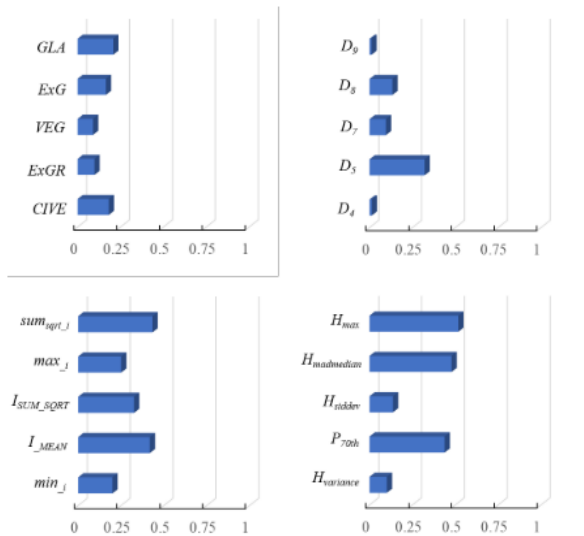

Ranking of correlation of feature variables

Experiment A

- ✓ Point cloud variables
- ✓ Vegetation index

Experiment B

- ✓ Point cloud variables
- ✓ Vegetation index
- ✓ HIS intensity variables

Experiment C

- ✓ Point cloud variables
- ✓ Vegetation index
- ✓ RGB intensity variables

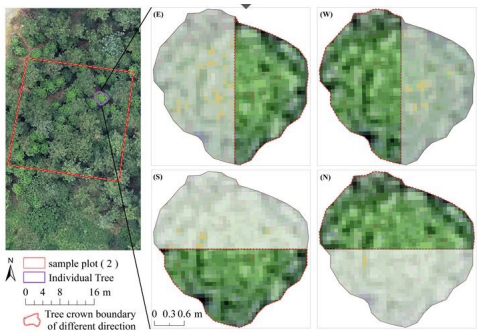

- ➢ Point cloud features were the dominant features. Both density and height variable correlations are high;
- ➢ Better intensity features, significantly better than spectral features;

Lei, L.; Chai, G.; Wang, Y.; Jia, X.; Yin, T.; Zhang, X. Estimating Individual Tree Above-Ground Biomass of Chinese Fir Plantation: Exploring the Combination of Multi-Dimensional Features from UAV Oblique Photos. Remote Sensing 2022, 14, doi:10.3390/rs14030504.

Forest parameter estimation

Individual tree crown parameters extraction using terrestrial close-range scanning and photogrammetry technology

- Terrestrial laser scanning
- Close-range photogrammetry sequence images

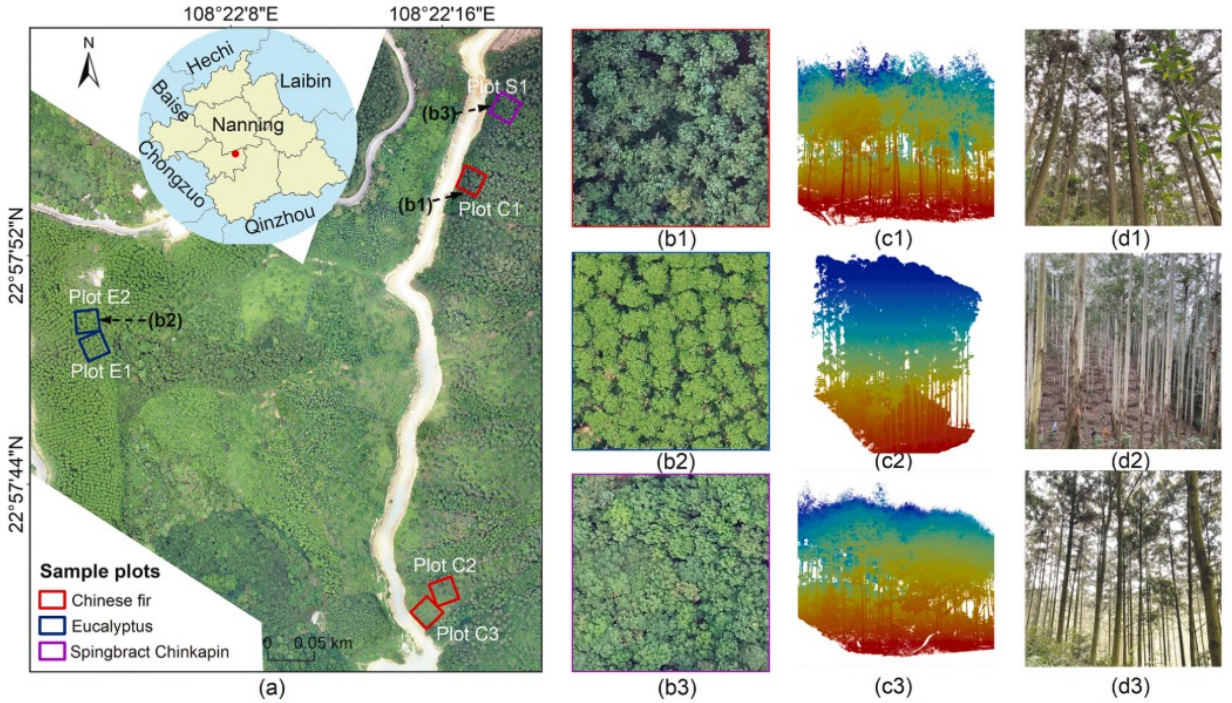

- Eucalyptus
- Chinese fir
- Spingbract Chinkapin

Forest parameter estimation

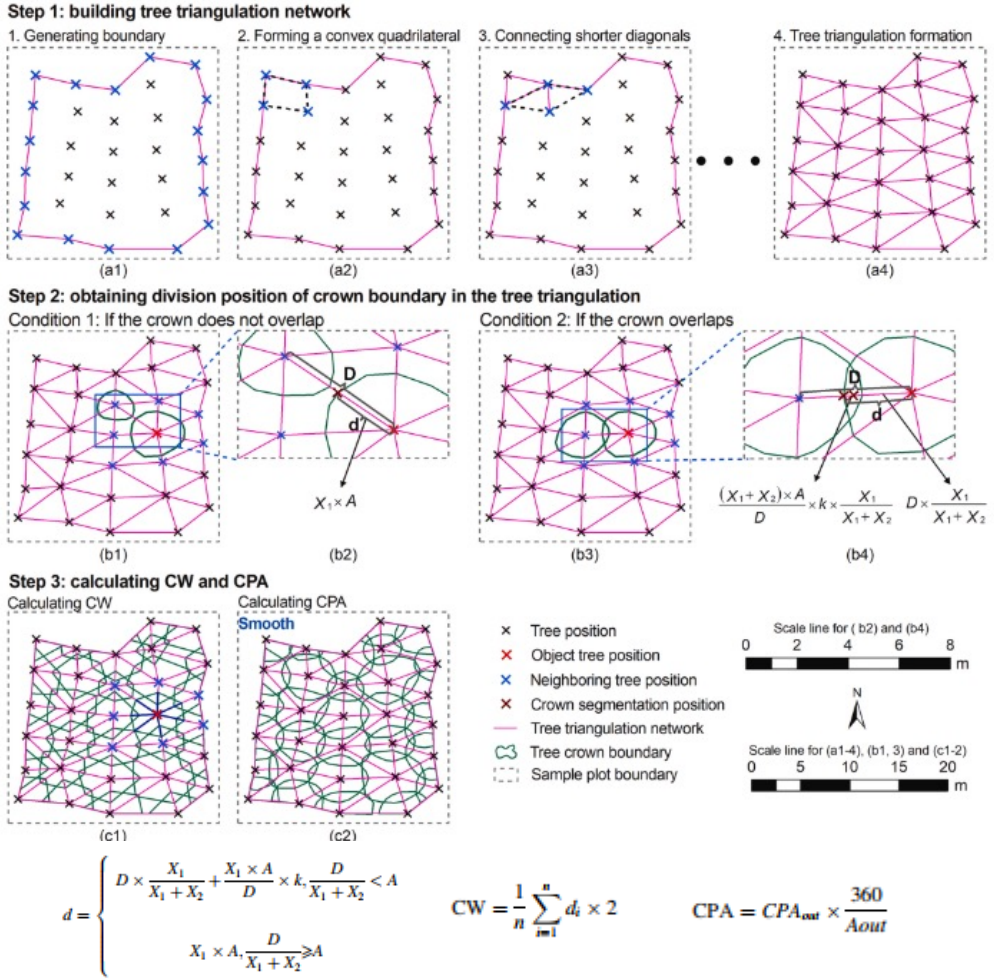

$$d=\begin{cases} D\times\frac{X_1}{X_1+X_2}+\frac{X_1\times A}{D}\times k,\frac{D}{X_1+X_2}<A \\ X_1\times A,\frac{D}{X_1+X_2}\geq A \end{cases}$$

$$CW=\frac{1}{n}\sum_{i=1}^{n}d_i\times 2 \qquad CPA=CPA_{out}\times\frac{360}{Aout}$$

- Considering spatial distribution characteristics of trees in actual forest scenes and the inter-tree growth competitive relationships.
- Considering accessibility of competition factors and their matching with TCRO data.

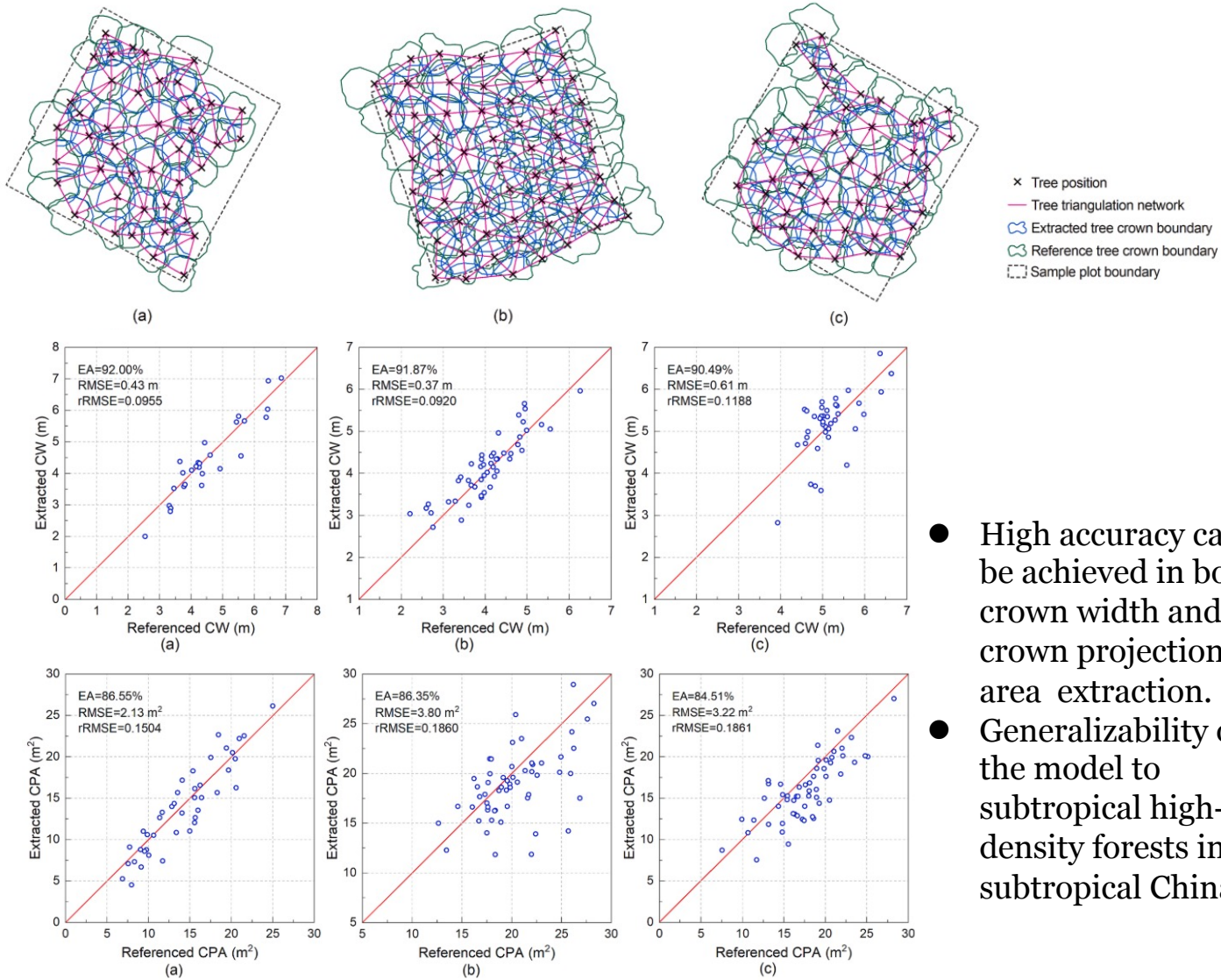

- High accuracy can be achieved in both crown width and crown projection area extraction.
- Generalizability of the model to subtropical high-density forests in subtropical China

Chai G., Zheng Y., Lei L., Yao Z., Chen M., Zhang X. A novel solution for extracting individual tree crown parameters in high-density plantation considering inter-tree growth competition using terrestrial close-range scanning and photogrammetry technology. Computers and Electronics in Agriculture, 2023, 209: 107849.

Forest parameter estimation

Forest tree height and biomass estimation using multi-source data

- ZY-3 stereo images
- Sentinel-2 multispectral image
- ALOS DEM dataset

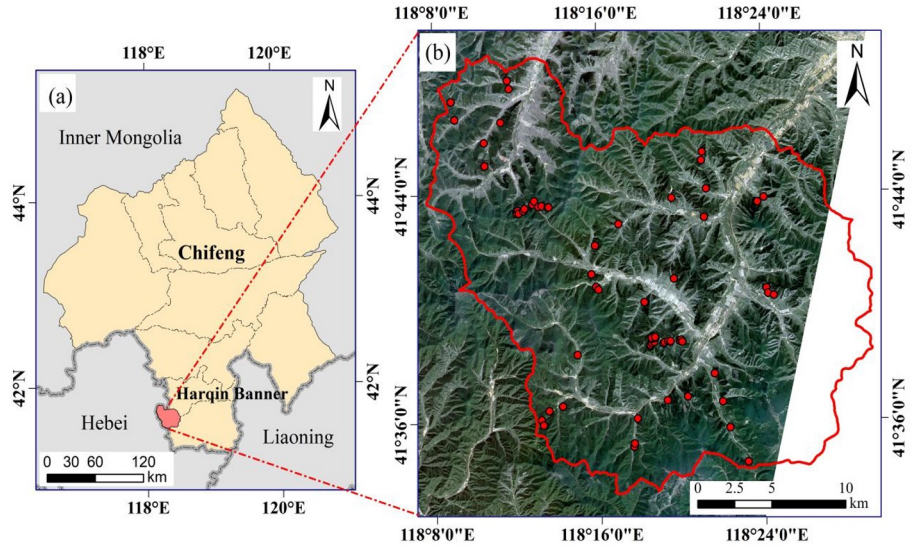

Location of the study area (a) and the distribution of the sample plots (b).

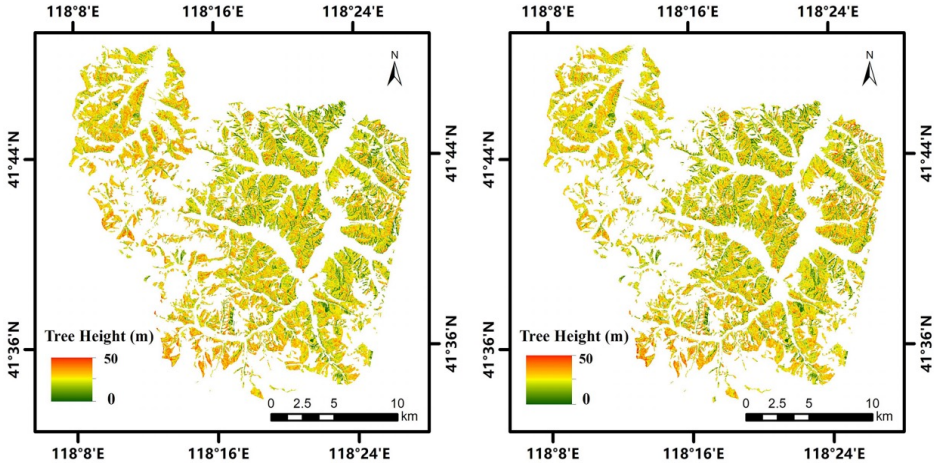

the nadir and forward views

the nadir and backward views

- The nadir and forward views provide better results than the nadir and backward views.
- A high-resolution wall-to-wall forest height map.
- By incorporating the tree height information, the AGB estimation can be significantly improved.
- **The data saturation problem can be alleviated.**

Yueting Wang, Xiaoli Zhang, Zhengqi Guo. Estimation of tree height and aboveground biomass of coniferous forests in North China using stereo ZY-3, multispectral Sentinel-2, and DEM data[J]. Ecological Indicators, 126.

Forest parameter estimation

A joint active-passive remote sensing point-line-polygon framework for regional forest aboveground biomass estimation

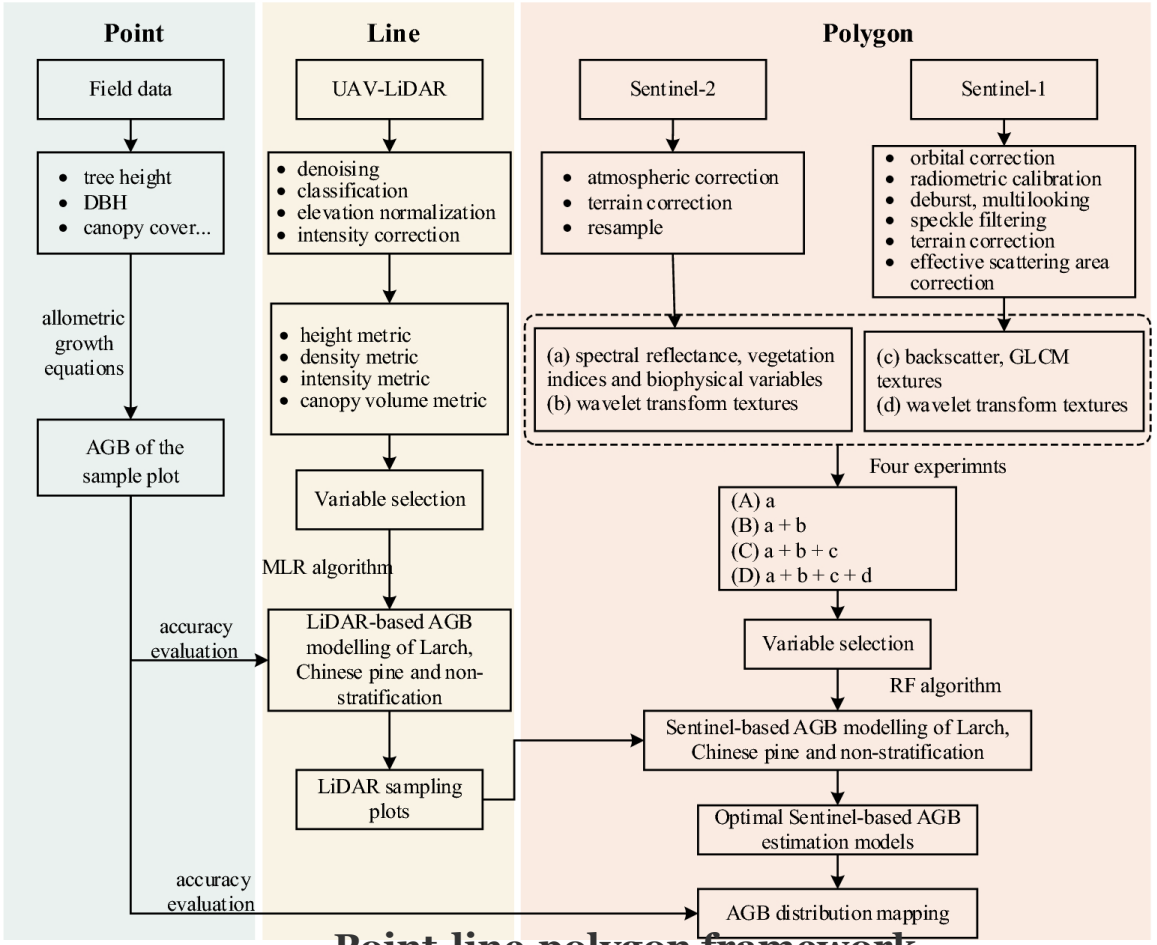

Point-line-polygon framework

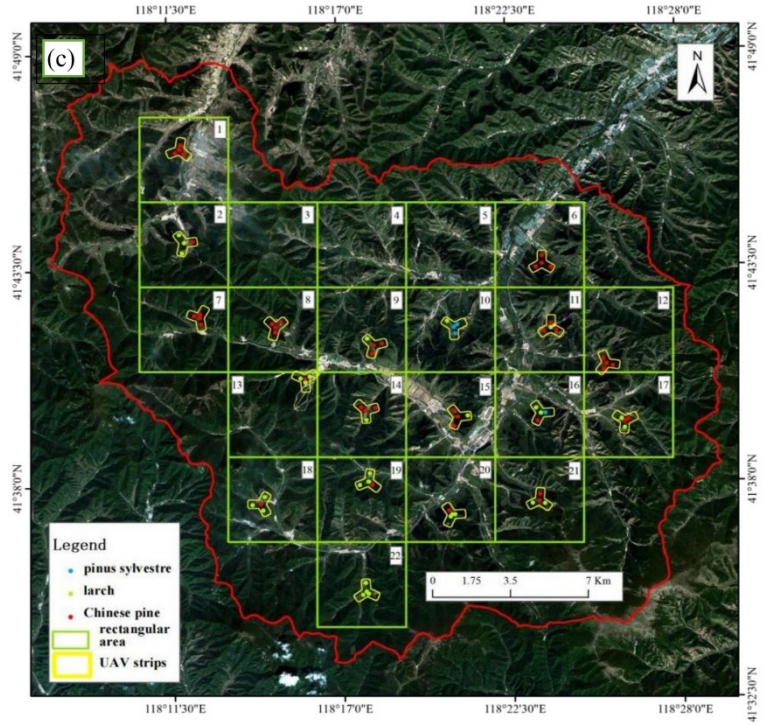

- The Point-line-polygon framework fully utilizes the respective strengths of UAV LiDAR, satellite-borne optics, and SAR data
- High-density LiDAR strip data can be used as a sample plot sampling tool to enable augmentation of sample plot data; a bridge for scale conversion
- Introducing the frequency domain and deep features of satellite-borne imagery to effectively mitigates the problem of spectral signal saturation in AGB estimation
- The point-line-polygon framework can achieve high-precision estimation and mapping of forest AGB on a large scale and can be used to assess regional forest carbon stocks.

Wang Y., Jia X., Chai G., Lei L., Zhang X. Improved estimation of aboveground biomass of regional coniferous forests integrating UAV-LiDAR strip data, Sentinel-1 and Sentinel-2 imageries. Plant Methods, 2023, 19(1): 65.

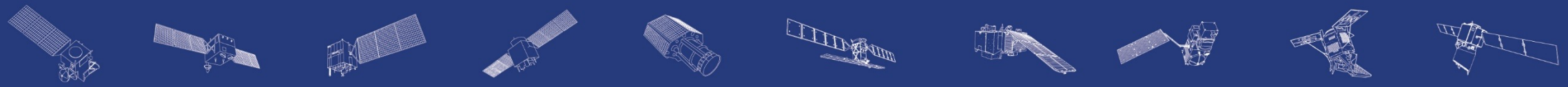

Forest Damage Detection

Beijing Forestry University

Swedish University of Agricultural Sciences

Monitoring of Pine Wilt Disease caused by pinewood nematode

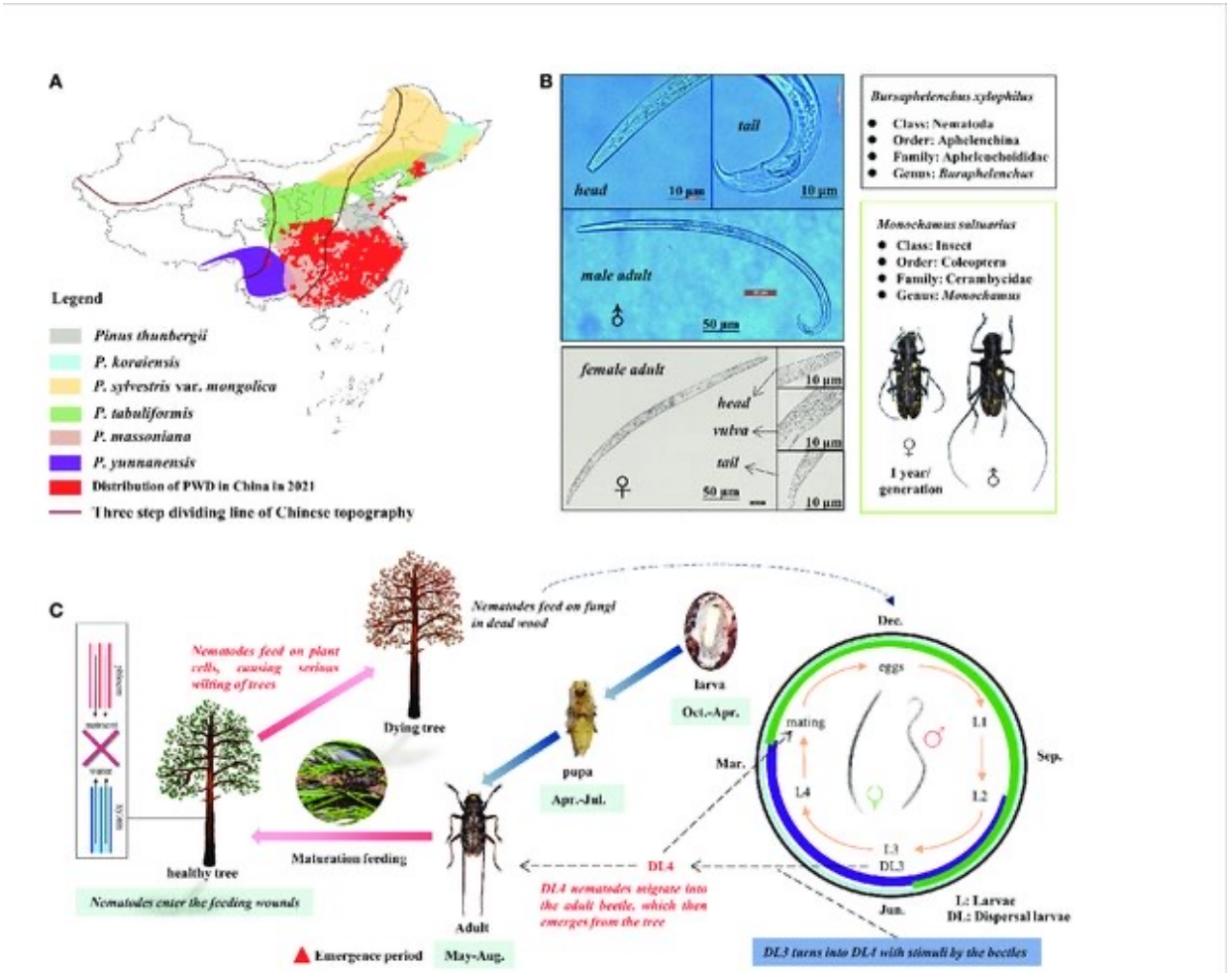

on of pine wilt disease in China in 2021 (A), morphology of *Monochamus saltuarius* and *Bursaphelenchus xylophilus* (B), and pathogenic m of pine wilt disease (PWD) (C).

Yu R. et, al., 2022, Early detection of pine wilt disease tree candidates using time-series of spectral signatures, Front. Plant Sci., 13 October 2022, Volume 13 - 2022 | https://doi.org/10.3389/fpls.2022.1000093

Forest Insect Damage Detection

European spruce bark beetle (*Ips typographus* [L.])

- Most destructive forest insects in Sweden and Europe

Image from https://www.skogsstyrelsen.se/bruka-skog/skogsskador/insekter/granbarkborre/

photo: Marek Matecki/CILP

Bark-beetle damaged forest in Germany.

Photo: BMEL.de

Figure

Caption

Figure 2. Norway spruce trees killed by the spruce bark beetle, Austria, Northern Front Range of the Alps. Photo: Rupert Seidl.

Forest Insect Damage Detection

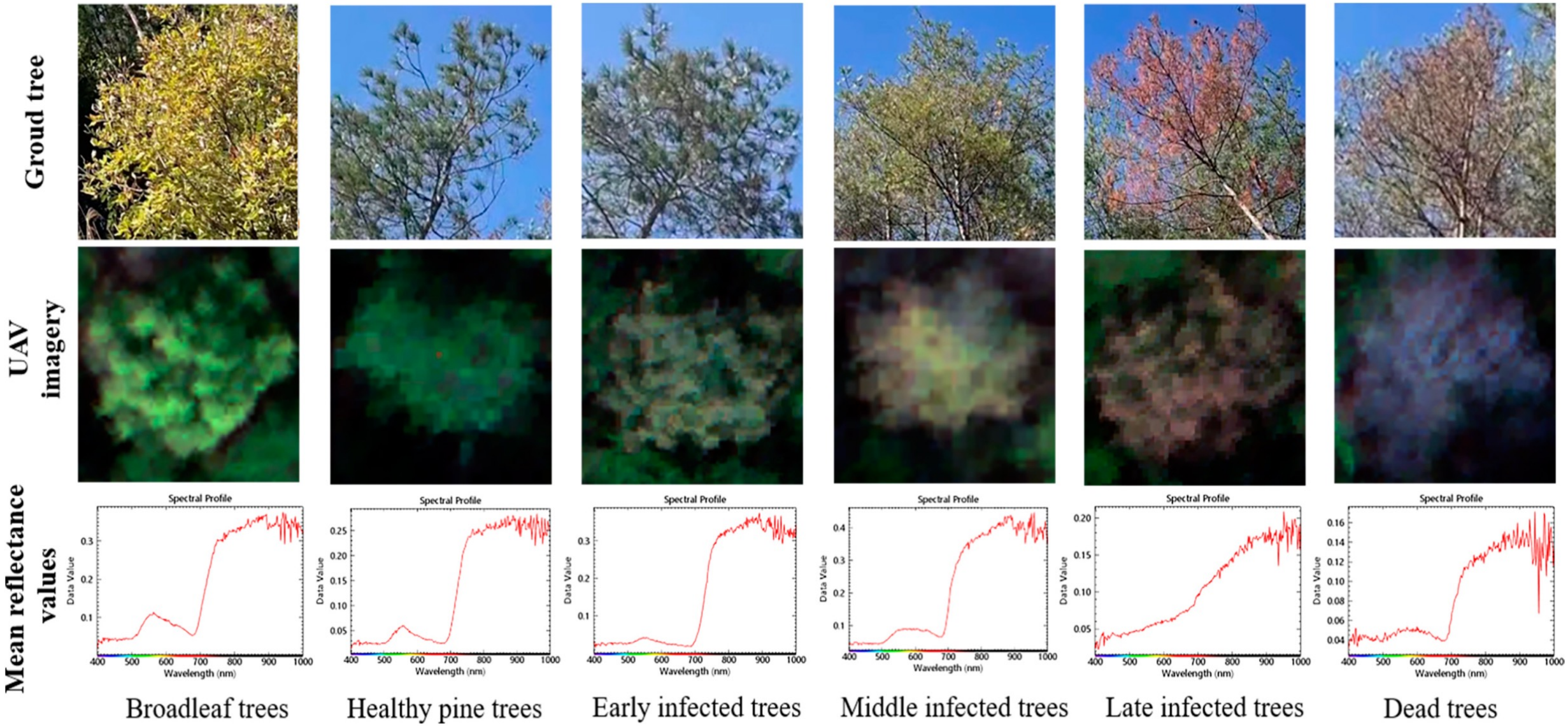

Monitoring of Pine Wilt Disease

- At the needle level

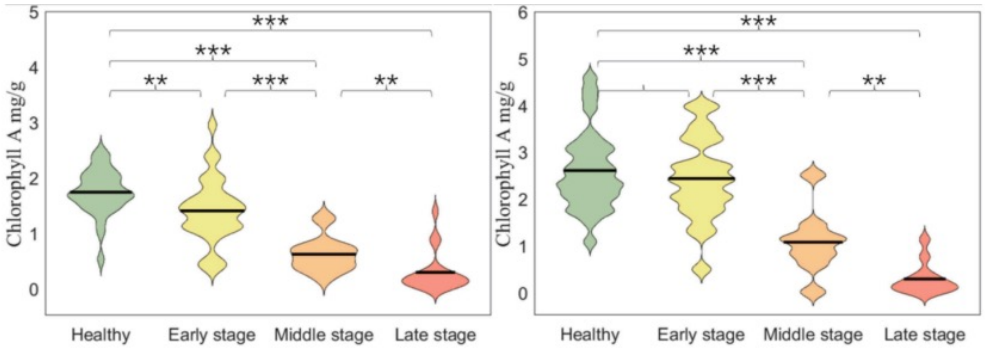

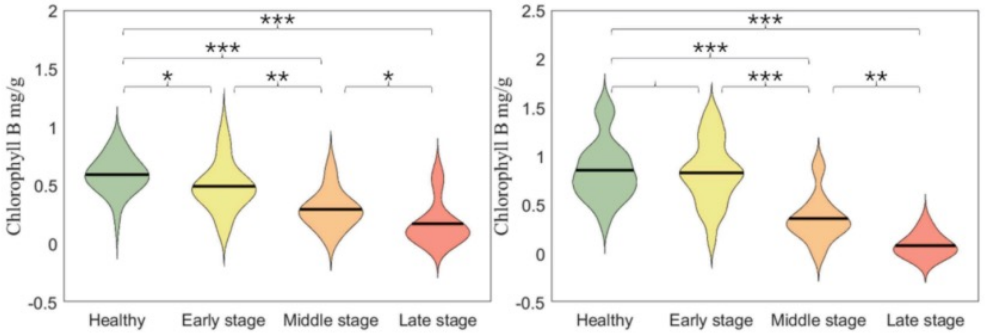

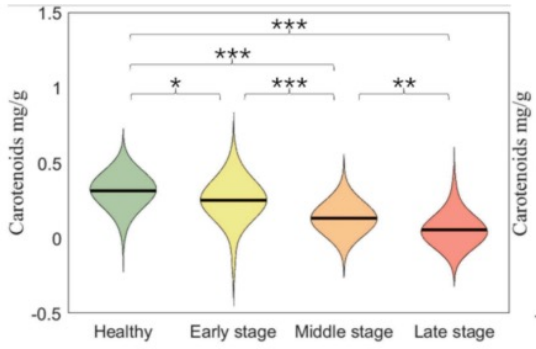

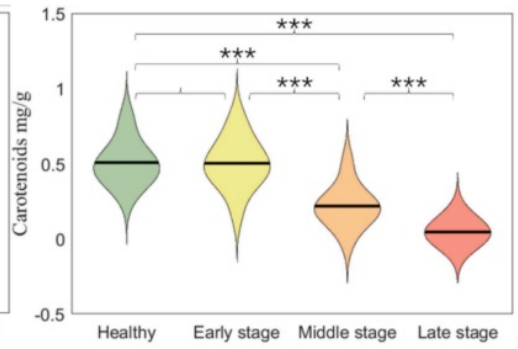

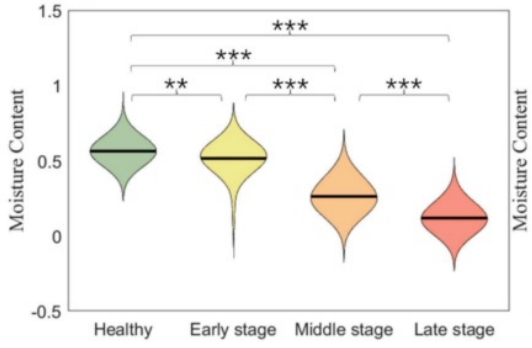

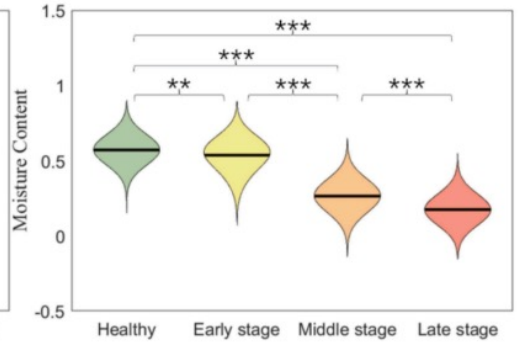

Niwen Li, Langning Huo, Xiaoli Zhang. Classification of pine wilt disease at different infection stages by diagnostic hyperspectral bands[J]. Ecological Indicators, 2022, 142: 109198.

Monitoring of Pine Wilt Disease

- At the needle level

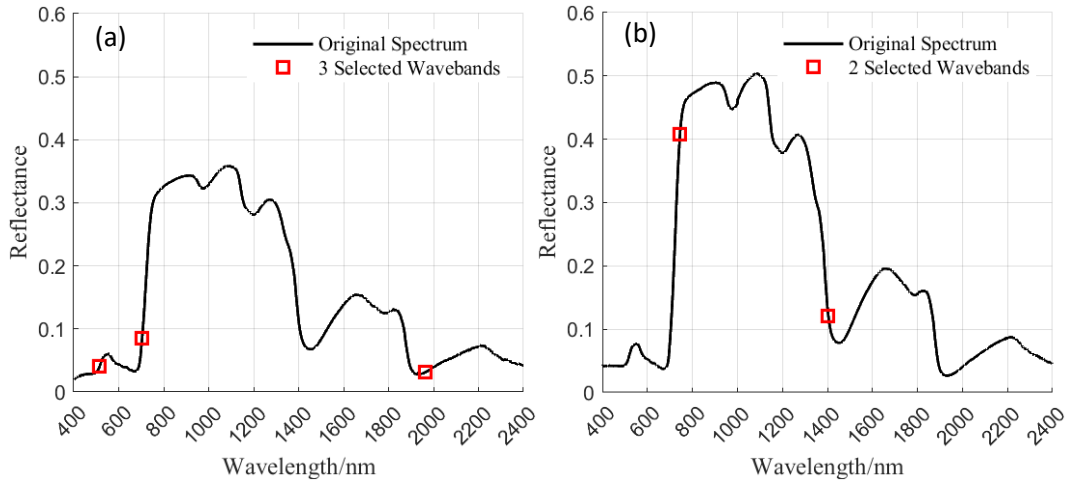

Figure. The sensitive bands of Japanese pine (a), Korean pine (b) selected by CARS-SPA.

Modeling method	Band select Algorithm	Modeling algorithm	Number of bands selected	Validation set				
				H	E	M	L	Total
Japanese pine	All bands	SVM-Linear	2001	0.82	0.58	1.00	0.89	0.78
		SVM-Polynomial	2001	0.73	0.83	1.00	0.56	0.75
		SVM- RBF	2001	0.27	0.42	1.00	0.78	0.53
	SPA	LDA	6	0.73	0.63	0.85	0.83	0.75
	CARS	LDA	15	0.70	0.63	0.79	0.79	0.72
	CARS-SPA	LDA	3	0.85	0.58	0.83	0.90	0.77
Korean pine	All bands	SVM-Linear	2001	0.91	0.75	0.40	1.00	0.79
		SVM-Polynomial	2001	0.27	0.88	0.40	1.00	0.57
		SVM- RBF	2001	0.82	0.63	0.00	1.00	0.64
	SPA	LDA	12	0.85	0.60	0.73	0.71	0.74
	CARS	LDA	14	0.75	0.67	0.76	0.88	0.74
	CARS-SPA	LDA	2	0.86	0.65	0.82	0.87	0.78

Table. Classification accuracy of Japanese pine and Korean pine samples using different selected bands and all bands. H, E, M, L represent the classes of healthy, early-, middle-, and late-stage infected samples.

Niwen Li, Langning Huo, Xiaoli Zhang. Classification of pine wilt disease at different infection stages by diagnostic hyperspectral bands[J]. Ecological Indicators, 2022, 142: 109198.

Monitoring of Pine Wilt Disease

- Individual tree level using hyperspectral drone images

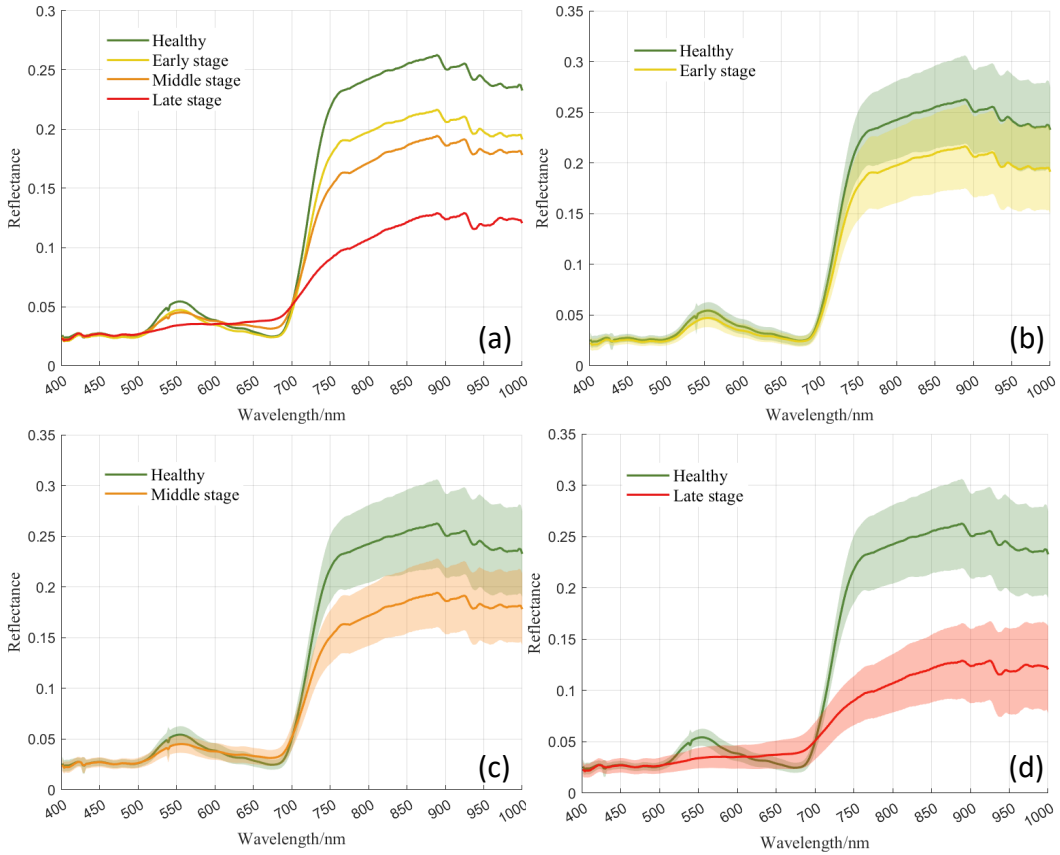

Figure. Mean spectral signature of tree crowns indifferent health status (a) and comparison between healthy and infected trees on the mean and standard deviation (std) of spectral signatures (b - d).

Niwen Li, Xiaoli Zhang, Langning Huo. Identifying nematode-induced wilt using hyperspectral drone images and assessing the potential of early detection. IGARSS 2022.

Monitoring of Pine Wilt Disease

- Individual tree level using hyperspectral drone images
  - Band selection
    - Bands with higher separability among healthy and early infected trees
    - Bands as Sentinel-2 images
  - Derivative reflectance
  - Vegetation indices
- Results and conclusions
  - Using first derivatives at 712 nm obtained 78.4% accuracy
  - Using red and blue edge inflection points obtained 73.8% accuracy
  - Using vegetation indices obtained up to 75% classification accuracy

Li, N. Research on Early Diagnostic Spectral Features of Pine Wilt Disease Based on Satellite-Airborne-Ground Remote Sensing Data. Ph.D. Thesis, Beijing Forestry University, Beijing, China, 2023

Forest Insect Damage Detection

Monitoring of Pine Wilt Disease

- Intelligent recognition of PWD-infected individual trees Using UAV-Based Hyperspectral Imagery
- Combining a prototypical network classification model with an individual tree segmentation algorithm

Categories	Mask R-CNN			Prototypical Network		Prototypical Network + Segmentation	
	RGB	Hyperspectral Full Bands	Feature Preferred Bands	Hyperspectral Full Bands	Feature Preferred Bands	Hyperspectral Full Bands	Feature Preferred Bands
OA (%)	64.60	68	71	92.17	92.79	82.95	83.51
AA (%)	64.58	68	70.98	91.33	93.46	82.20	84.11
Kappa	0.574	0.582	0.596	0.889	0.898	0.800	0.808
E	54.30	62.90	63.50	82.17	83.21	73.95	74.89
M	73.10	72.70	77.50	93.87	92.54	84.48	83.29
L	62	64.50	68.40	95.82	97.61	86.24	87.85
D	68.90	71.90	74.50	93.71	97.6	84.34	87.84

Figure . PWD infection stage diagnosis.

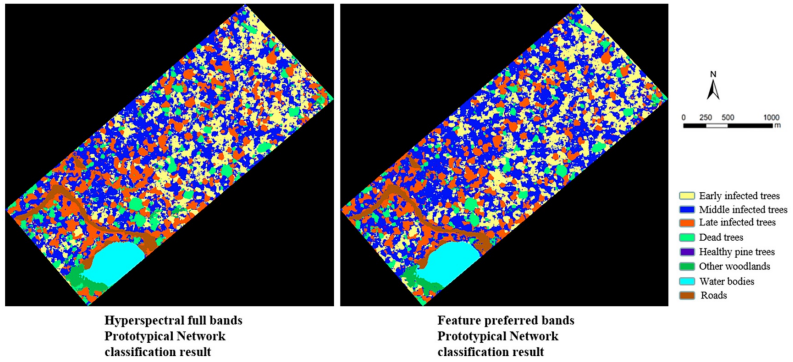

Figure . Prototypical network classification result map.

Li, H.; Chen, L.; Yao, Z.; Li, N.; Long, L.; Zhang, X. Intelligent Identification of Pine Wilt Disease Infected Individual Trees Using UAV-Based Hyperspectral Imagery. Remote Sens. 2023, 15, 3295. https://doi.org/10.3390/rs15133295

Forest Insect Damage Detection

Monitoring of Pine Wilt Disease

- NDFI: A new vegetation index for mapping coniferous forest.
- A new monitoring model of the PWD infection stage was built using Machine learning algorithm.

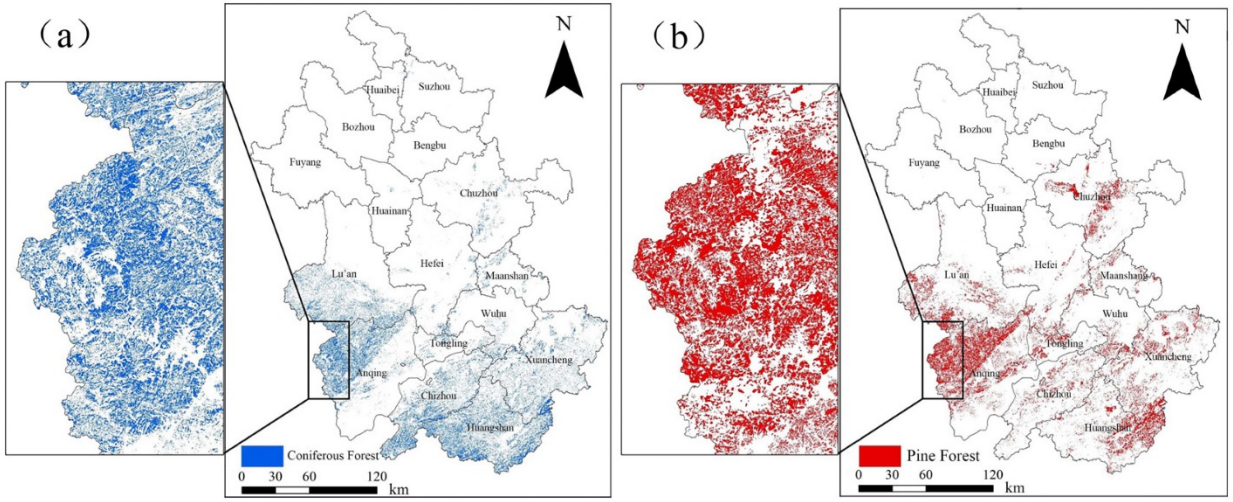

Figure. Comparison of the extracted coniferous forest area and the distribution area of pine forest sub-compartments.(a) Area of coniferous forest extracted in this paper. (b) Area of coniferous forest in Forest Management Inventory.

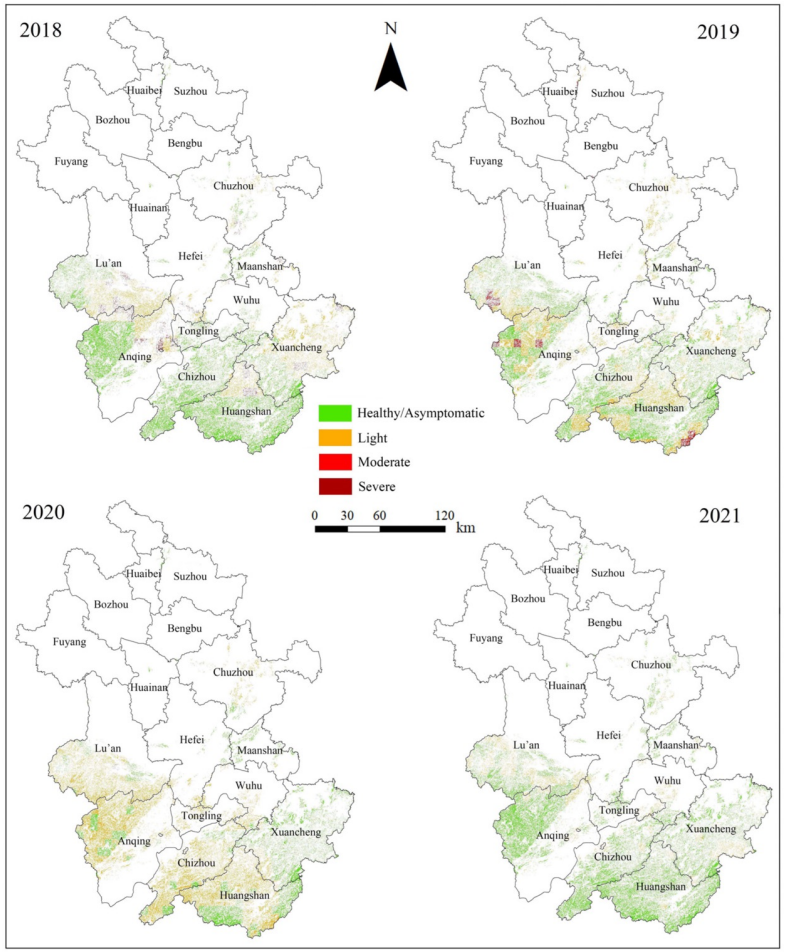

Figure. Grading map of PWD degree from 2018 to 2021.

Long, L., Chen, Y., Song, S., Zhang, X., Jia, X., Lu, Y., & Liu, G. (2023). Remote Sensing Monitoring of Pine Wilt Disease Based on Time-Series Remote Sensing Index. Remote Sensing, 15, 360


一风起绿浪
共赴山海
林业生物质能源研究所
蓝莓研究发展中心
草地生态与资源研究中心
林业应对气候变化研究所
高尔夫教育与研究中心
草坪研究所
城市林业研究中心
测绘与3S技术中心

Forest Insect Damage Detection

Monitoring of European Spruce Bark Beetles

- Early detection and large area mapping using Sentinel-2 images

- A new vegetation index (NDRS) was proposed to map the bark beetle damages.
- Spectral differences were observed before attacks

$$DRS = \sqrt{(Red)^2 + (SWIR)^2}$$

$$NDRS = \frac{DRS - DRS'_{min}}{DRS'_{max} - DRS'_{min}}$$

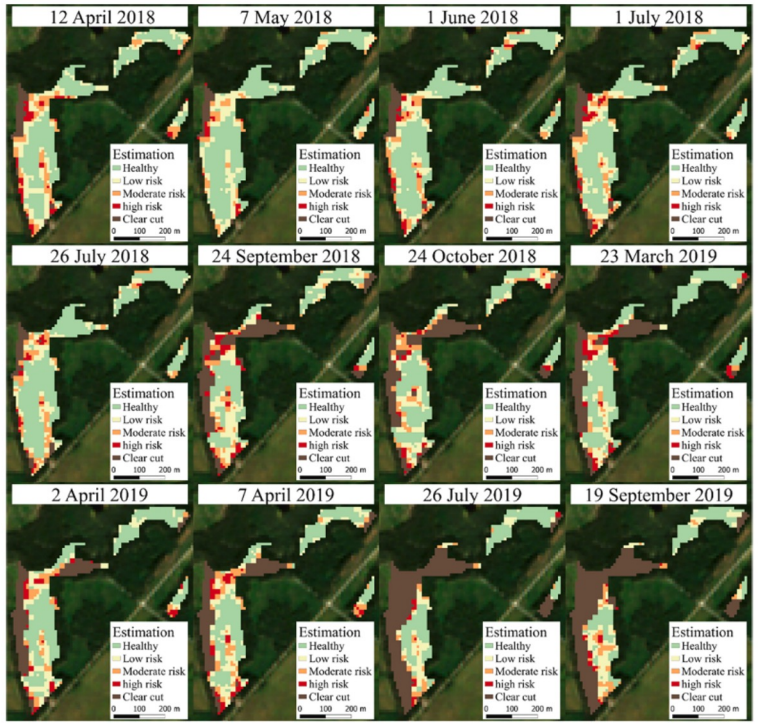

Fig. A5. A case study showing estimated attacks in a time-series and the spatial spread pattern of bark beetle infestations.

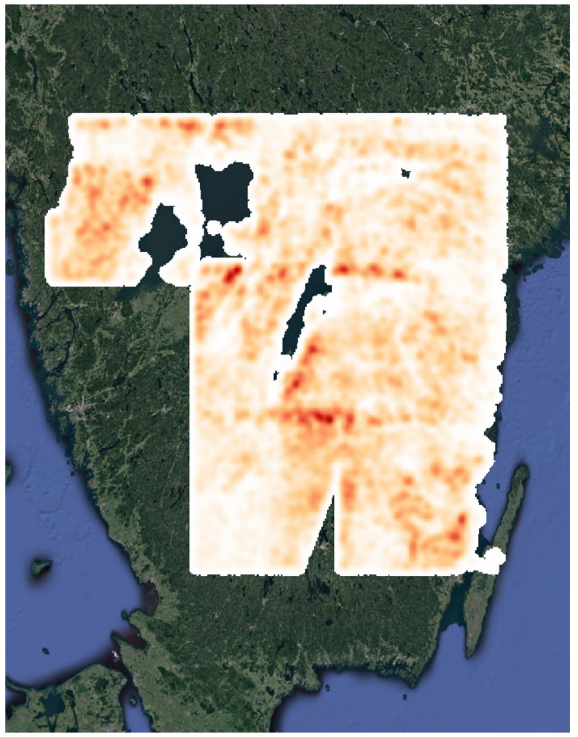

Huo L, Persson H, Lindberg E., 2021. Early detection of forest stress from European spruce bark beetle attack, and a new vegetation index: Normalized Distance Red & SWIR (NDRS). Remote Sensing of Environment, 255, 112240.

Monitoring of European Spruce Bark Beetles

- Operational large-area bark beetle mapping

- The Distance Red & SWIR index was tested to map the bark beetle damages in one Sentinel-2 tile (110×110 km²).
- Validation using harvester data, covering 11,786 pixels (10×10 m²), 842 attacked and 137 healthy tree clusters.
- An overall accuracy of 78% on classifying attacked and healthy clusters using the change of DRS.

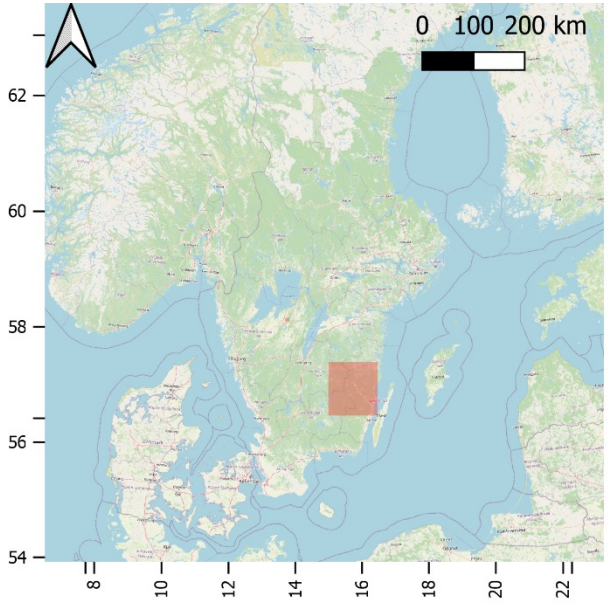

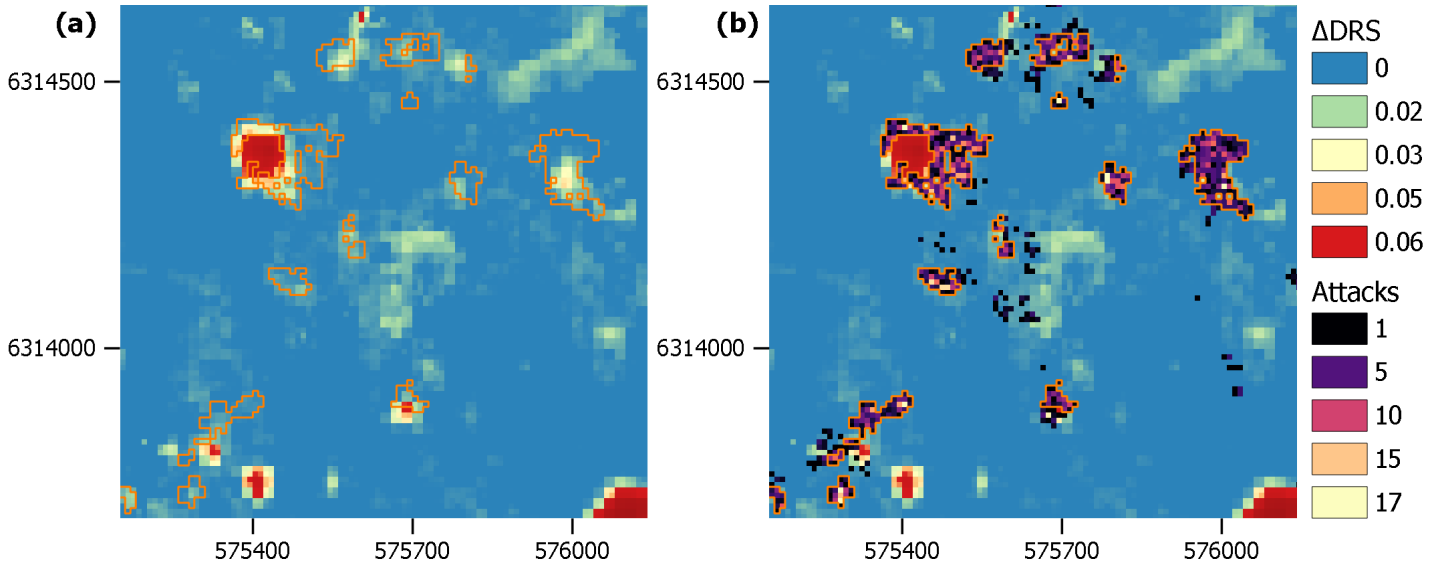

Persson, H., Huo, L., Lindberg, E., & (manuscript). Using the distance red swir index – DRS –with Sentinel-2 satellite images for operational large-area bark beetle mapping

Something interesting……

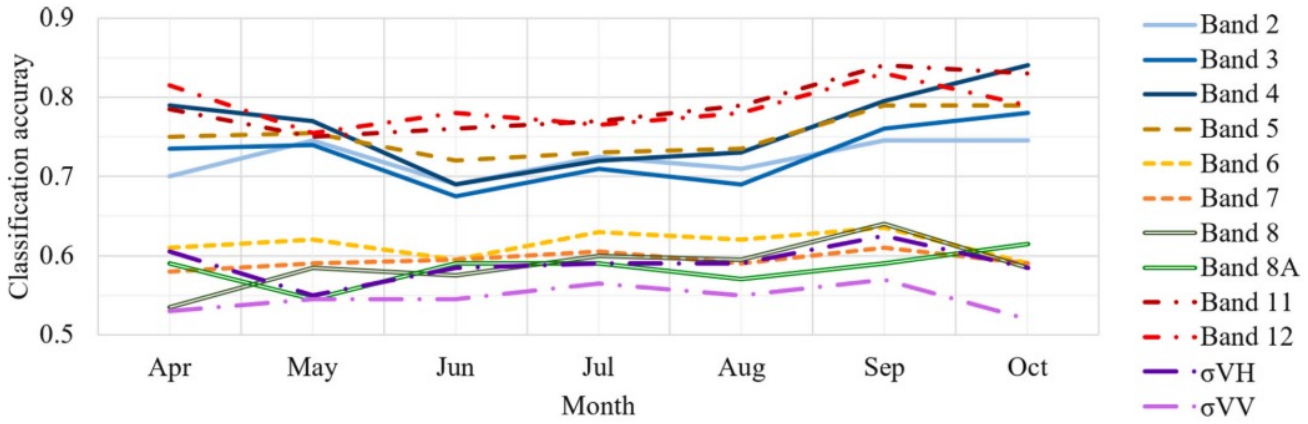

Fig. 8. Separability of individual bands shown by using CA from LDA and leave-one-out cross-validation.

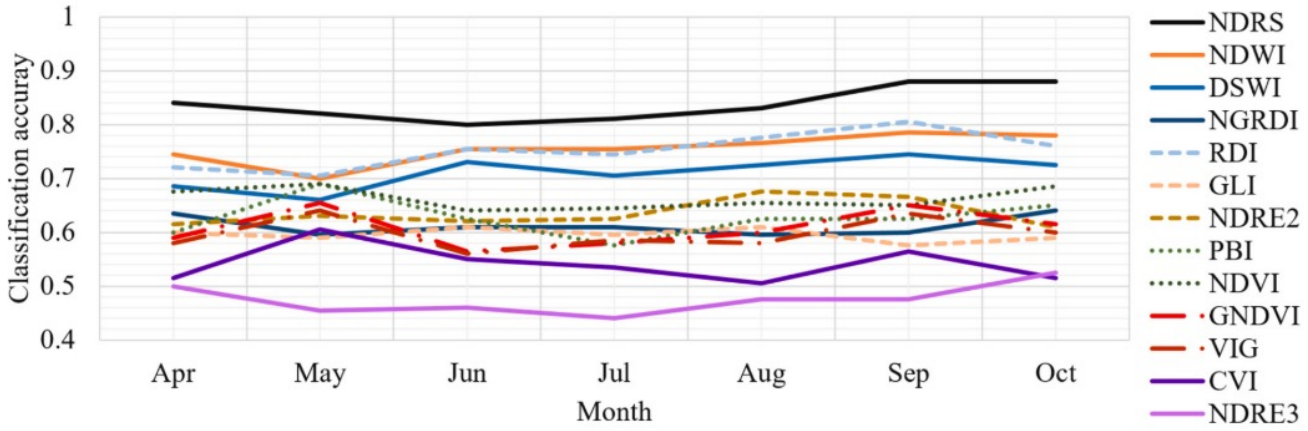

Fig. 9. Separability of vegetation indices for stress detection shown by CA from LDA and leave-one-out cross-validation.

Forest Insect Damage Detection

Monitoring of European Spruce Bark Beetles

- Is green-attacks detectable using satellite images?

- Sentinel-2

  The number of attacked trees limited the time of detection

  - Attacks with >20 trees showed abnormal spectral before attacks.
  - Attacks with >10 trees can be identified in August.
  - Attacks with 5-10 trees can be identified in September.
  - Attacks with <5 trees cannot be identified.

- WorldView-3 SWIR

  No significant differences in June

  - Too early in the infestation stage
  - Shadow effects

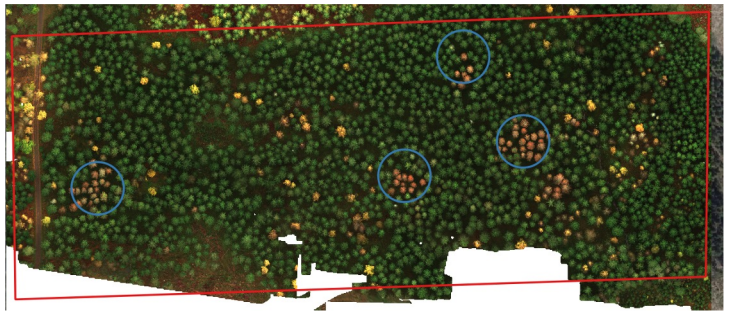

A drone image

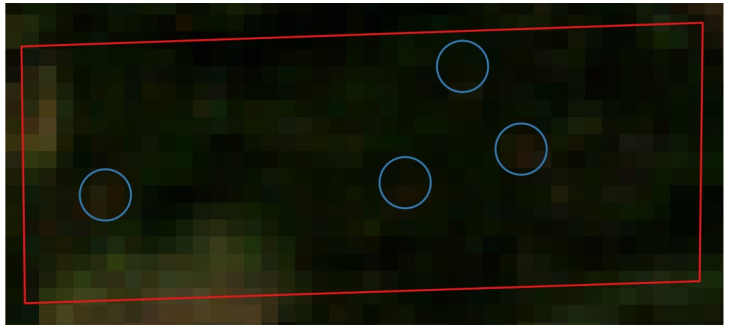

A Sentinel-2 image

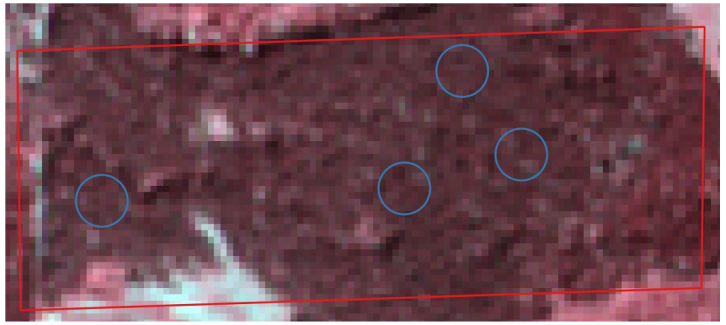

A WorldView-3 SWIR image

Huo, L., Lindberg, E., Fransson, J.E.S., & Persson, H.J. (2022). Comparing Spectral Differences Between Healthy and Early Infested Spruce Forests Caused by Bark Beetle Attacks using Satellite Images. In IGARSS 2022 IEEE International Geoscience and Remote Sensing Symposium (pp. 7709–7712): IEEE.

A controlled experiment

- 977 spruces were monitored
- 208 spruces were attacked
- The first swarm started in week 20 (May 17), with 155 trees attacked.
- The second swarm started in week 30 (July 26), with 53 trees attacked.
- Drone flights in May, June, August, and October.

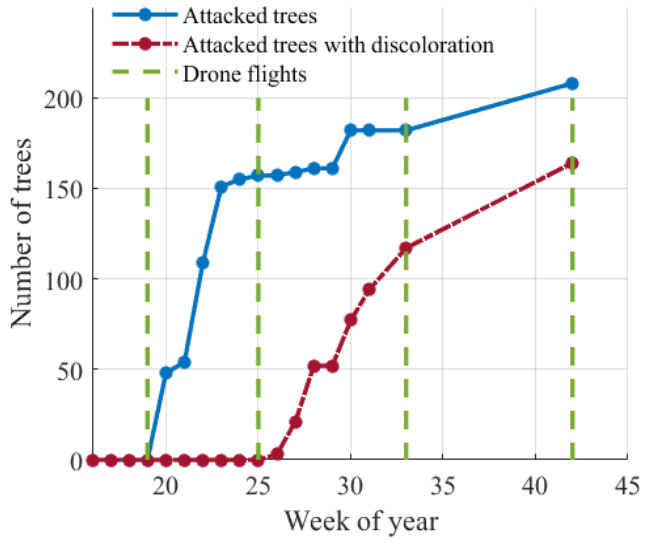

Drone image acquisition

- Multispectral drone images, 0.04 m pixels, 9 bands
- 80 m above the ground

Band no.	Color	Center wavelength (nm)	Bandwidth (nm)
1	Violet	443	20
2	Blue	490	65
3	Green	560	35
4	Red	665	30
5	Red-edge	705	15
6	Red-edge	740	15
7	NIR	783	20
8	NIR	842	115
9	NIR	865	20

Incident Light Sensor (ILS)

radiometric reference targets

DJI Matrice 210 RTK

MAIA S2 multispectral camera

Forest Insect Damage Detection

Early detection of European Spruce Bark Beetle attacks at the individual tree level

- Early detection using drone images

- Multispectral drone images were used with the same wavelengths of Sentinel-2.
- How early did the infested trees show abnormal spectra was investigated.
- The continuous changes of the detectability during green-attacks was quantified.

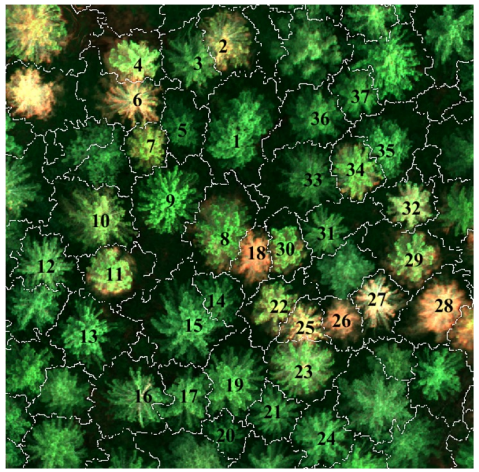

Segmentation of individual tree crowns in a drone image

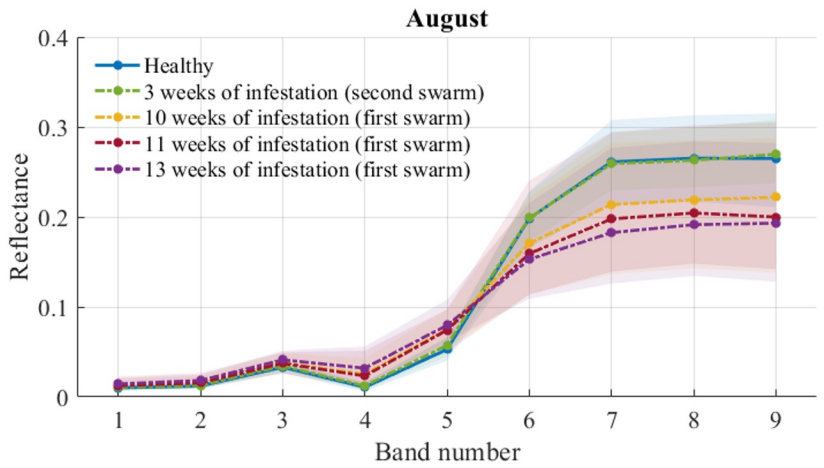

Spectral signatures of tree groups infested for different duration

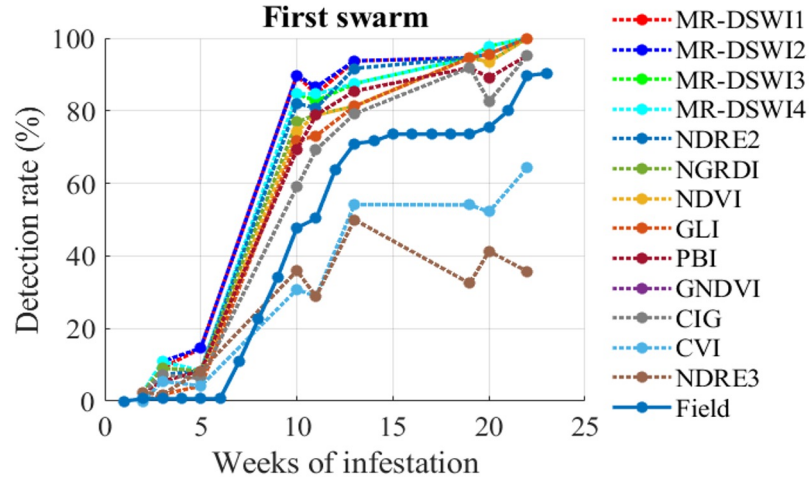

Detectability increased rapidly during 5 – 10 weeks of infestation

Huo, L., Lindberg, E., Bohlin, J., & Persson, H.J. (2023). Assessing the detectability of European spruce bark beetle green attack in multispectral drone images with high spatial- and temporal resolutions. Remote Sensing of Environment, 287, 113484.

Monitoring of European Spruce Bark Beetles

Machine learning & vegetation indices

- RF and LDA with multiple variables showed overfitting and low transferability on untrained area.
- Using single VIs showed higher accuracy and robustness.
- Testing on untrained area is crucial to show the transferability of a model.

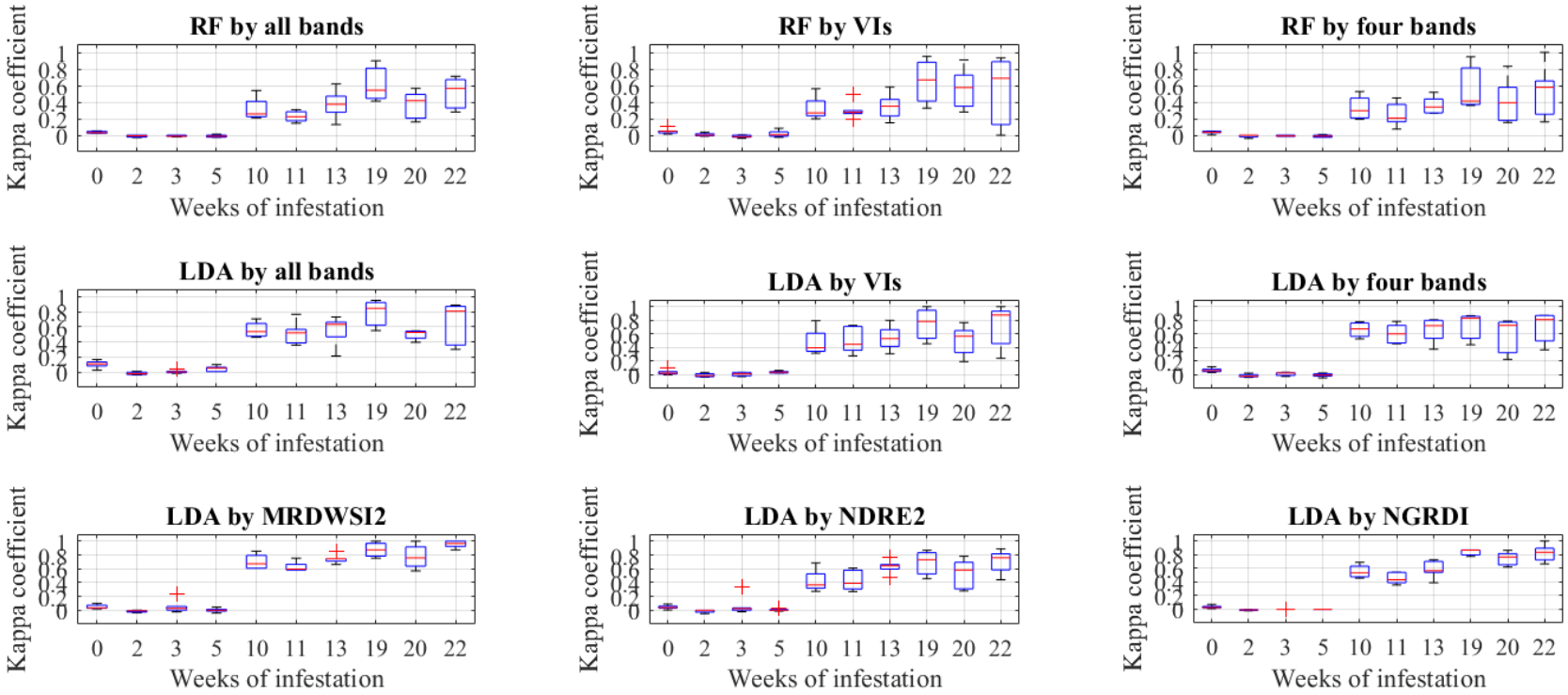

Huo, L., Persson, H.J., Bohlin, J., & Lindberg, E. (2023). Green-attack detection or Overfitting? Comparing Machine-learning- and Vegetation-index-based Methods to Early Detect European Spruce Bark Beetle Attacks Using Multispectral Drone Images. In IGARSS 2023 IEEE International Geoscience and Remote Sensing Symposium.

A drone with a hyperspectral camera

A drone flight mission for hyperspectral image acquisition

Stations monitoring sap flow changes during bark beetle attacks

Inventory of tree attributes

Recording the damages

Trees damaged by bark beetles shown on drone videos

Further research plan

- Explore the potential of **hyperspectral drone images** on the early detection of infestations.
- Implement and improve the method of **large-area forest damage mapping** using satellite images.
- Explore the spatial and temporal distribution patterns of forest disturbance in China using improved CCDC algorithm, and to study the characteristics of different disturbance factors and vegetation restoration mechanisms.

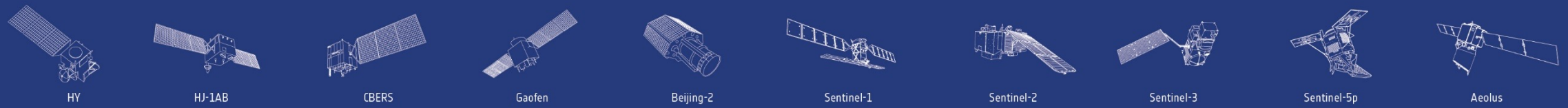

Mapping forest changes and tree species

Swedish University of Agricultural Sciences

TanDEM-X for Swedish test site

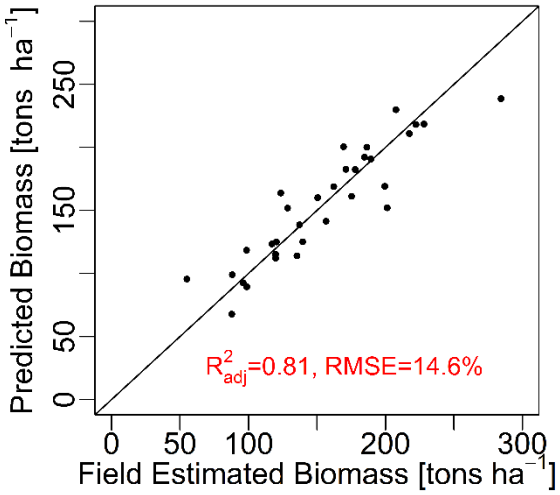

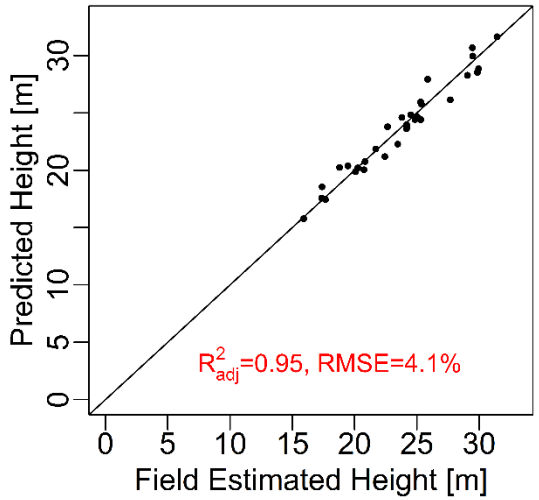

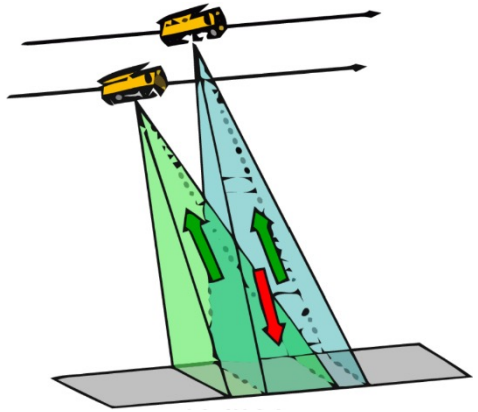

Estimations for thirty-two 0.5 ha plots in Remningstorp.

Test site	Variable	Date	R^2_{adj}	RMSE	n
Remningstorp	AGB	2011-06-04	0.81	1.1 tons/ha (14.6%)	32
Remningstorp	Height	2011-06-04	0.95	1.0 m (4.1%)	32

Comparison laser vs. radar based biomass map of Sweden

(Persson et al. 2017)

remote sensing

Article

Experiences from Large-Scale Forest Mapping of Sweden Using TanDEM-X Data

Henrik J. Persson [1,*], Håkan Olsson [2], Maciej J. Soja [2,3] and Lars M.H. Ulander [4]

[1] Swedish University of Agricultural Sciences (SLU), Department of Forest Resource Management, Umeå SE-90, Sweden; hakan.olsson@slu.se (H.O.); johan.fransson@slu.se (J.E.S.F.)
[2] Hexagon Geospatial, Luleå SE-97, Sweden
[3] School of Land and Food, University of Tasmania, Hobart, TAS 7001, Australia; maciej.soja@utas.edu.au
[4] Chalmers University of Technology, Department of Earth and Space Sciences, SE-412 96, Sweden; lars.ulander@chalmers.se
* Correspondence: henrik.persson@slu.se; Tel.: +46-90-786-8105

Received: 12 October 2017; Accepted: 29 November 2017; Published: 2 December 2017

Abstract: This paper reports experiences from the processing and mosaicking of 508 TanDEM-X image pairs covering the territory of Sweden, with two single map products of above-ground biomass (AGB) and forest stem volume (VOL), both with 50 m resolution. The main objective was to explore the possibilities and overcome the challenges related to forest mapping using a large number of adjacent satellite scenes. Hence, numerous examples are presented to illustrate challenges and possible solutions. To derive the forest maps, the observables backscatter, interferometric phase height and interferometric coherence, obtained from TanDEM-X, were evaluated using empirical robust linear regression models with reference data extracted from 2286 national forest inventory plots with a 10 m radius. The interferometric phase height was the single most important observable, to predict AGB and VOL. The resulting models were evaluated on different datasets with field-inventoried stands across Sweden. The root mean square error (RMSE) was about 25%–29% (37–50 tons/ha and 52–85 m³/ha). Because of this variability at the scene-level, determinations of AGB and VOL for single stands are recommended to be used with care, as an equivalent accuracy is difficult to achieve for all different scenes, with varying acquisition conditions. Still, for the evaluated stands, the models were of sufficient accuracy to be used for forest management at the stand level.

Keywords: TanDEM-X; forest; mosaic; synthetic aperture radar; volume; biomass; modelling

1. Introduction

The amount of remote sensing data of the Earth is increasing, and moreover, the quality of the collected data increases. For forest-related purposes, field inventories paired with airborne laser scanning (ALS) data have made forest maps of several vital variables, e.g., tree height, basal area, above-ground biomass (AGB) and stem volume (VOL), of yet unprecedented accuracy available [1–3]. AGB and VOL are strongly correlated, although AGB also includes the branches and is more commonly used in climate modelling, while the industry and forest owners tend to use VOL, as this is a metric of the merchantable forest products [4]. Airborne techniques (including photogrammetry) are both highly accurate, but also expensive for frequent usage, especially at larger scales. Satellite-based techniques have the advantage that they can cover large areas even across national borders and be repeated frequently at lower costs. National satellite-based forest maps with about 25 m resolution have been available in Sweden for almost two decades, and ongoing work to derive world-wide ground height

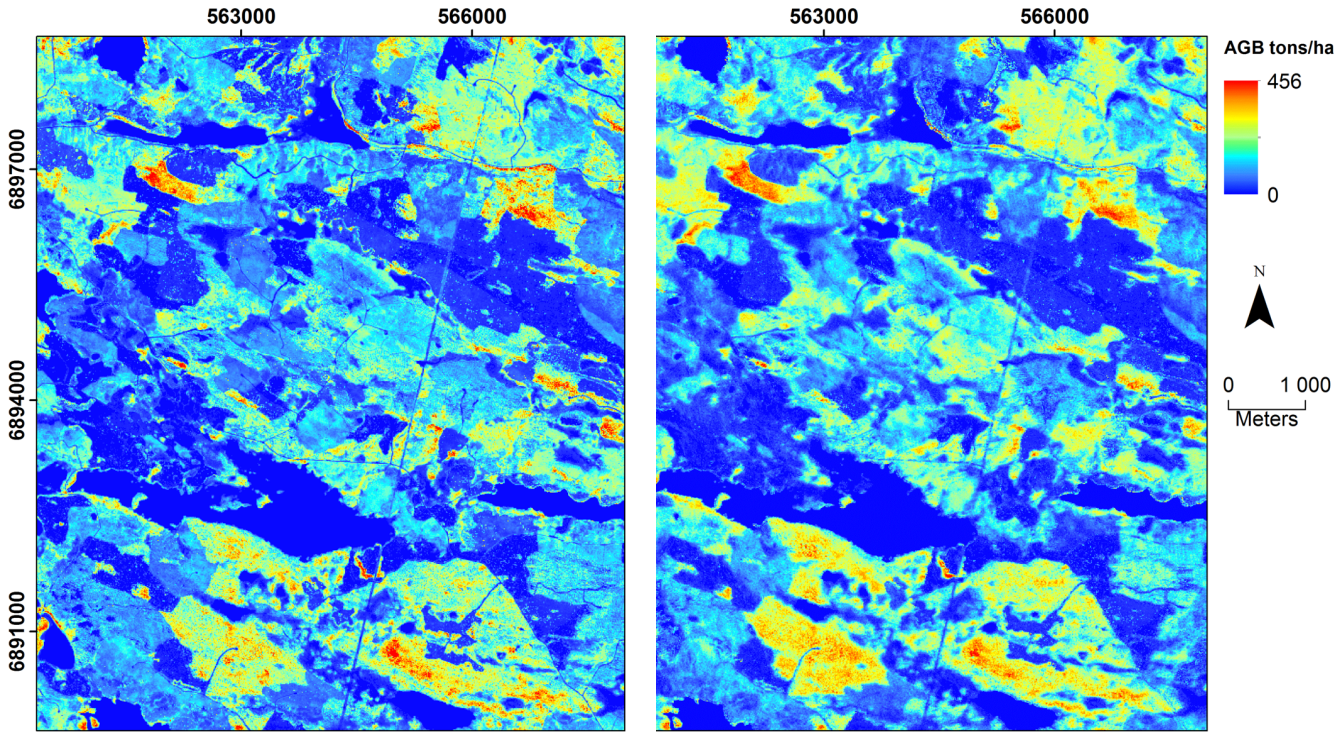

Airborne laser

TanDEM-X radar

RMSE **~19-22%** **~21-25%**

(compared to field inventory at stand-level)

Site index

- The soil's inherent capacity to produce wood volume
- Indirect measure of forest site productivity
- Determined from habitat elements, or tree height and age

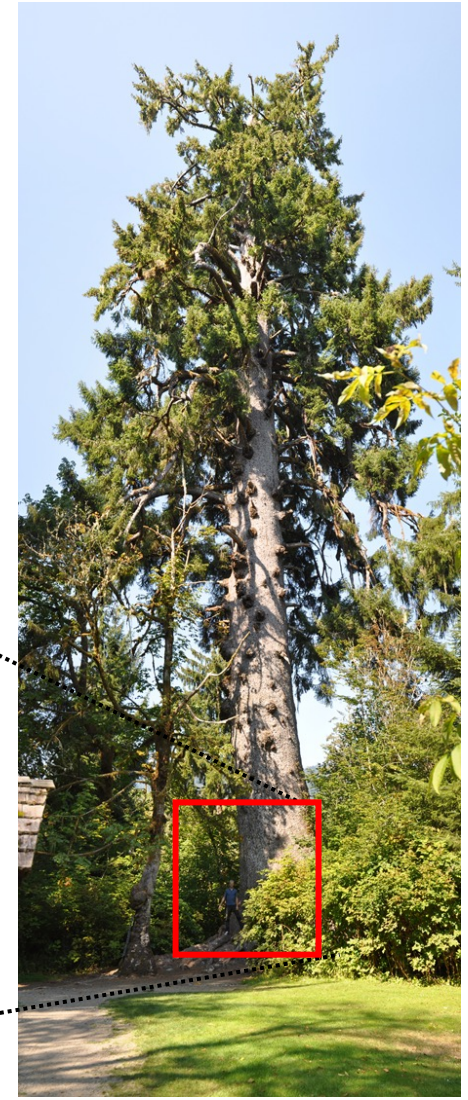

Determining SI from heights

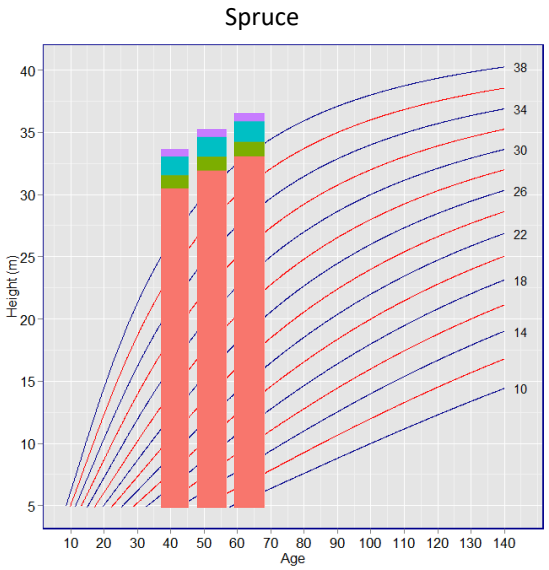

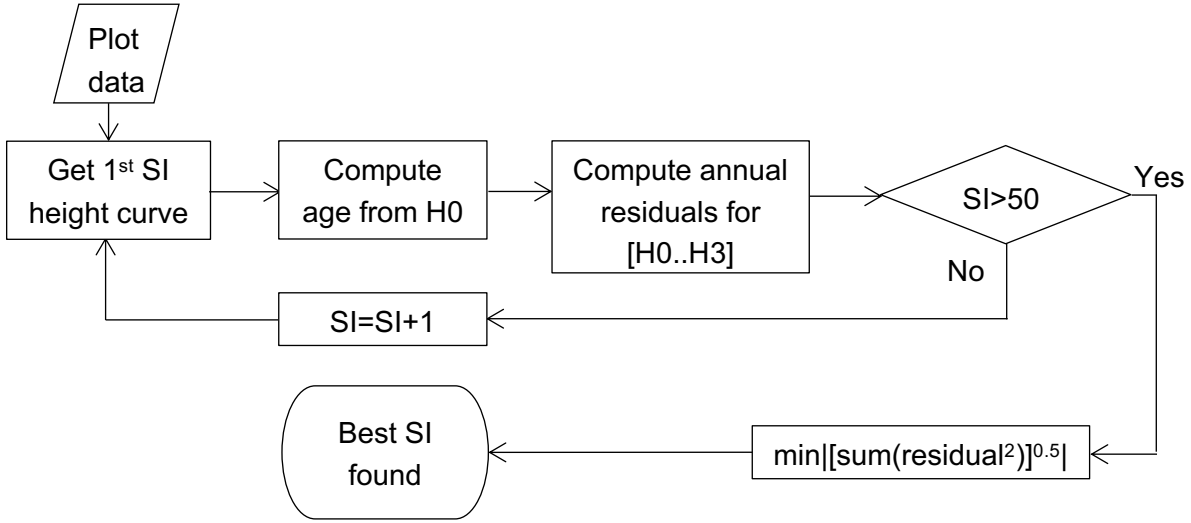

3598 IEEE JOURNAL OF SELECTED TOPICS IN APPLIED EARTH OBSERVATIONS AND REMOTE SENSING, VOL. 9, NO. 8, AUGUST 2016

Estimating Site Index From Short-Term TanDEM-X Canopy Height Models

Henrik J. Persson and Johan E. S. Fransson, *Senior Member, IEEE*

2016

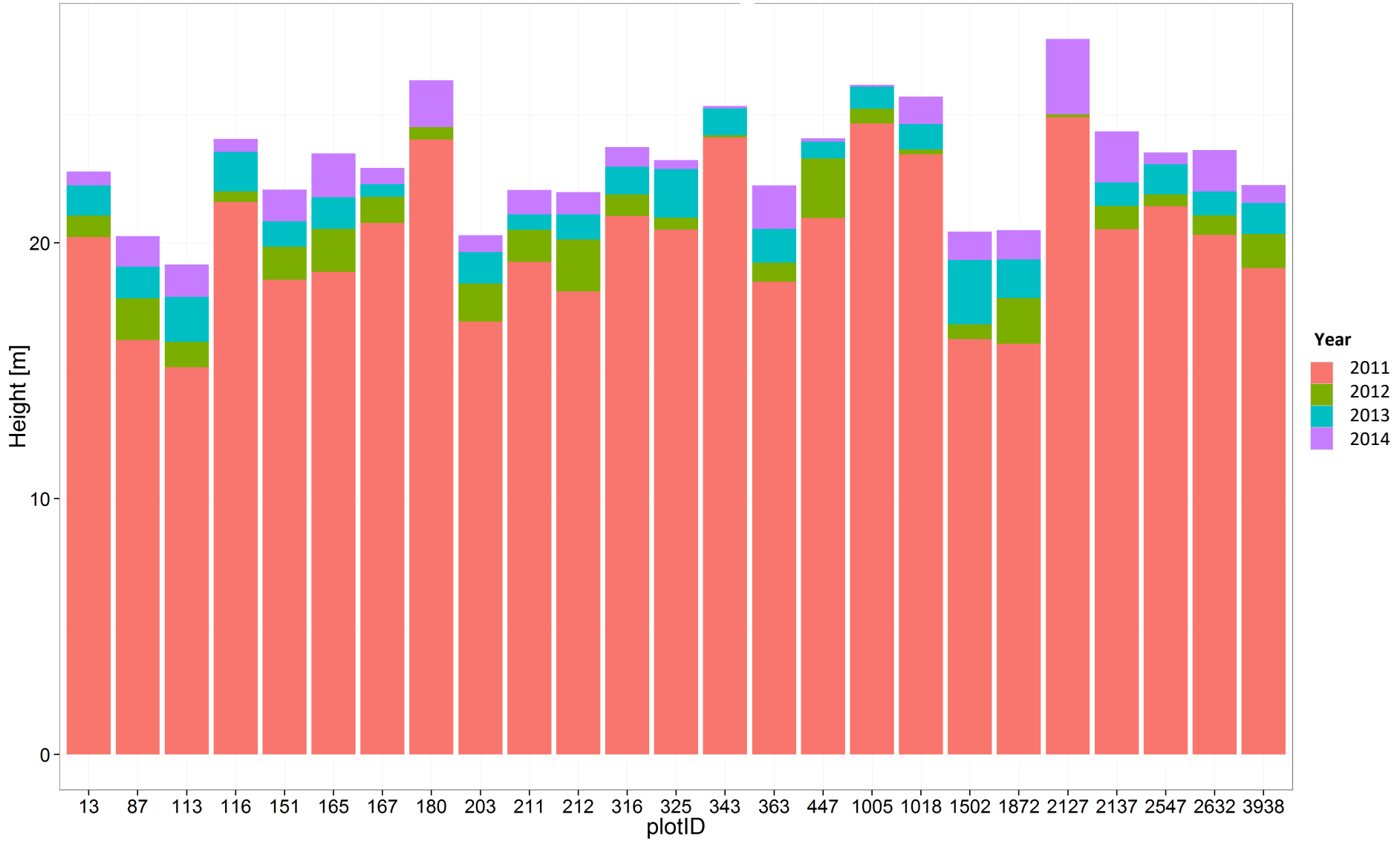

Forest parameter estimation

Treatment Detection Using InSAR Time Series

TanDEM-X (German Aerospace Center (DLR))

RS data

Time series of 24 VV polarization scenes. Aug 2011 - June 2014

Processed to obtain interferometric height using 2 m x 2 m DTM, final phase height products 10 m × 10 m in ground resolution.

Pixel level penetration depth correction: (ha: height of ambiguity, γ: coherence)

$$\Delta h = -\frac{|h_a|}{2\pi}\arctan\left(\sqrt{|\gamma|^{-2}-1}\right), \quad (1)$$

Field data

34 plots, 40m in radius. located inside homogenous stands.

Treatment records in forest management plan used to classify plots into 25 untreated, 5 thinned, and 4 clear-cut.

I. Huuva, H.J. Persson, J. Wallerman, and J.E.S. Fransson, "Detectability of Silvicultural Treatments in Time Series of Penetration Depth Corrected TanDEM-X Phase Heights," In *Proceedings of IGARSS 2022,* Kuala Lumpur, Malaysia

New study covering 7 seasons

- 30 TanDEM-X images
- 91 plots á 10 m radius
- RMSE 4.4 m (12.1%)

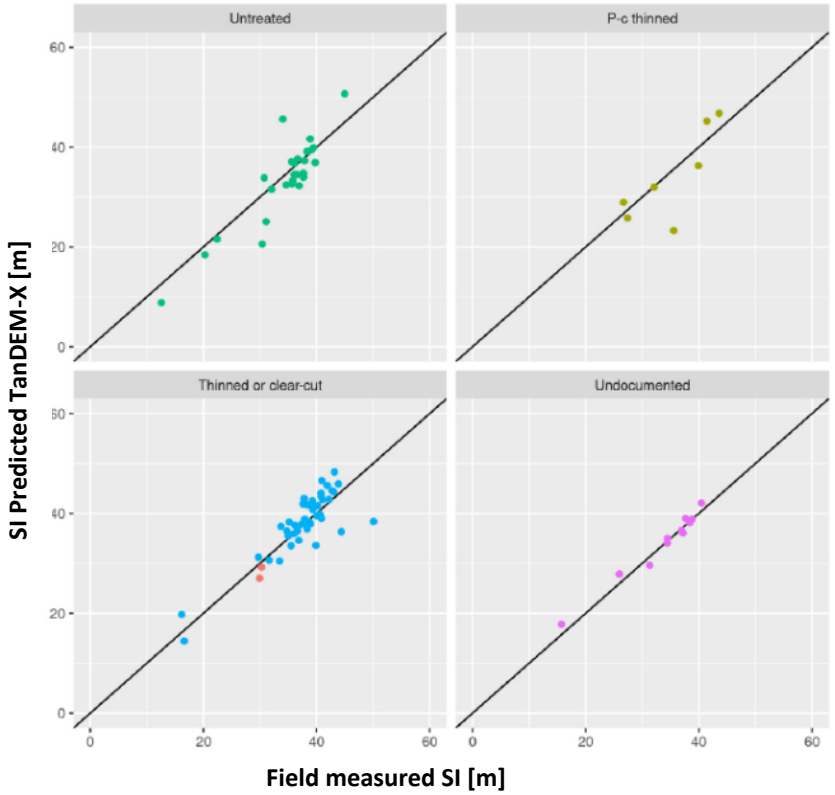

remote sensing
Aug 2023

Article

Prediction of Site Index and Age Using Time Series of TanDEM-X Phase Heights

Ivan Huuva [1,*], Jörgen Wallerman [1], Johan E. S. Fransson [2] and Henrik J. Persson [1]

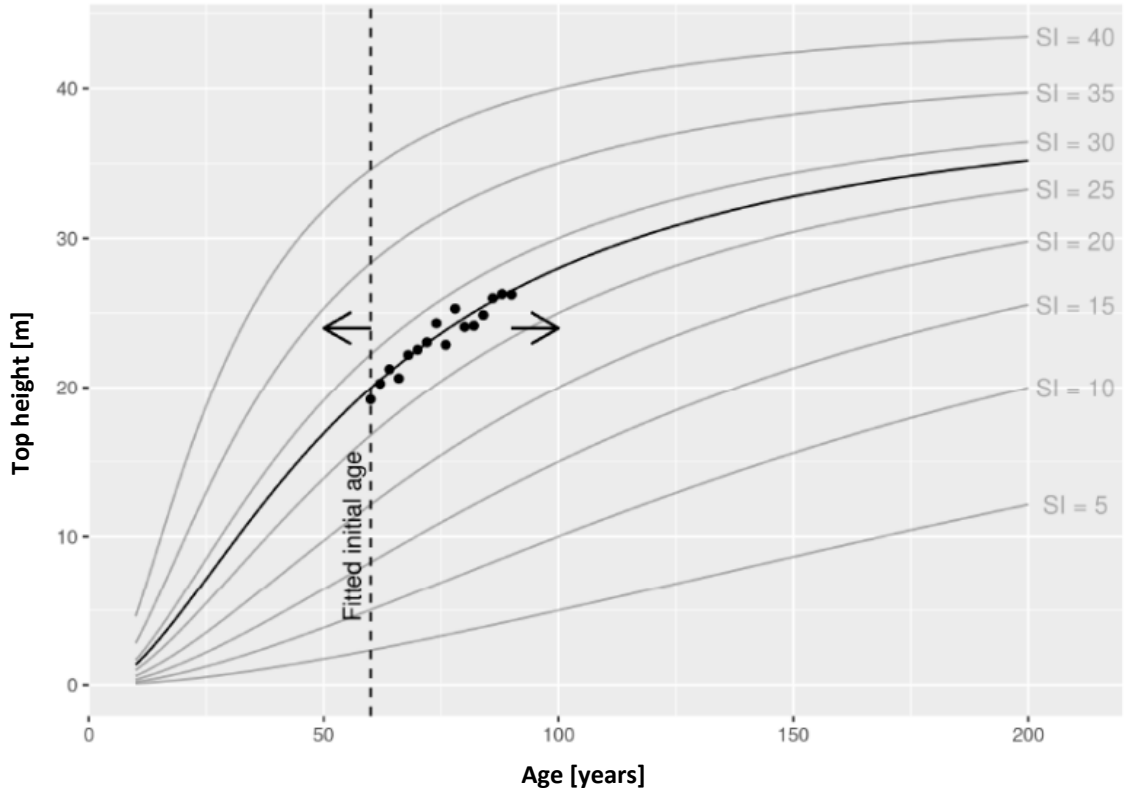

Forestry activities – 4 classes

- Untouched (no changes)
- Pre-commercial thinning (lower vegetation cut)
- Commercial thinning (~35% of basal area removed)
- Clear-cut (almost all trees removed)

Illustration: Nils Forshed

© Skogforsk · LRF Skogsägarna · Skogsstyrelsen

Forestry activities

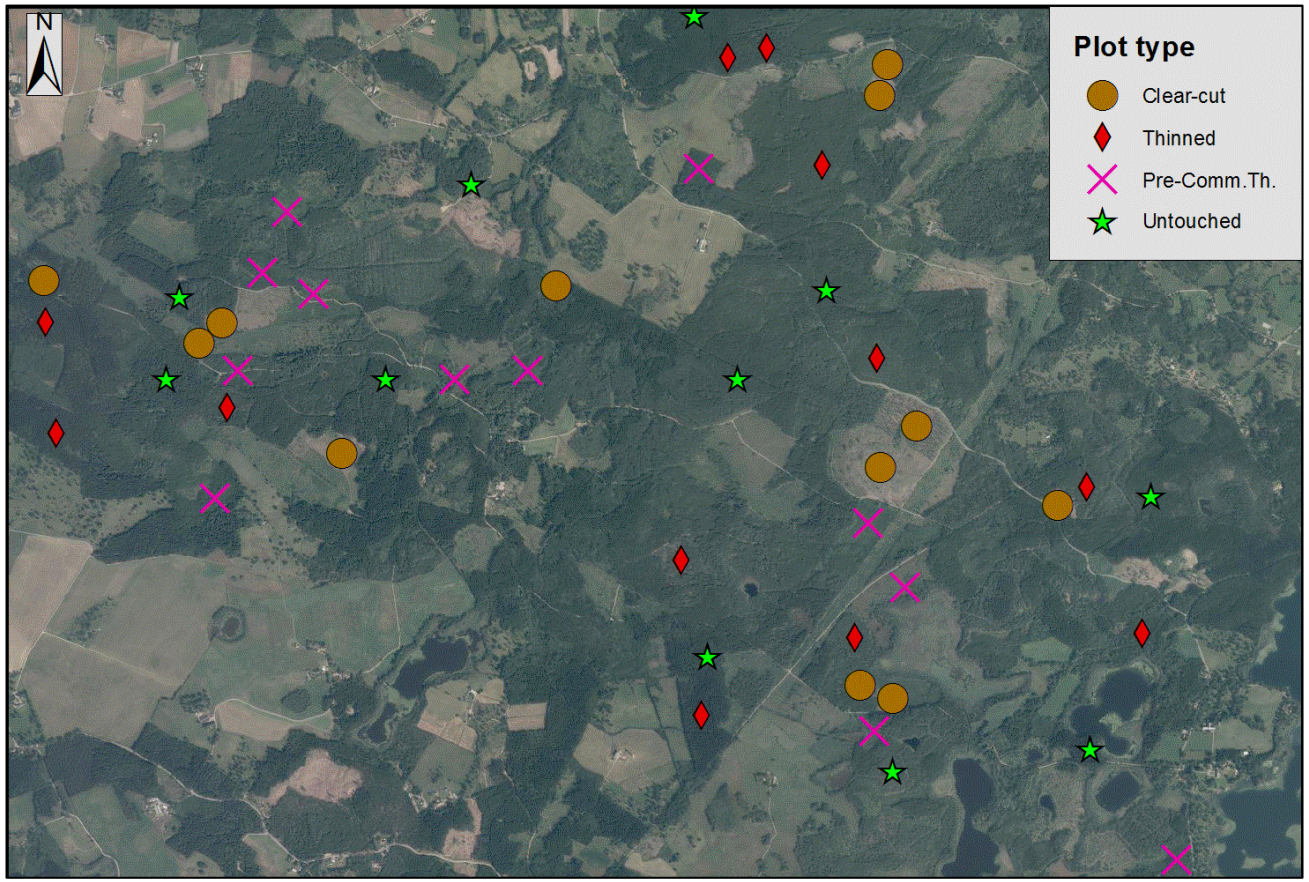

- 4 classes:
  - pre-commercial thinning
  - thinning
  - clear-cutting
  - unchanged
- 12 plots each, 40 m radius

Change of AGB from TanDEM-X InSAR

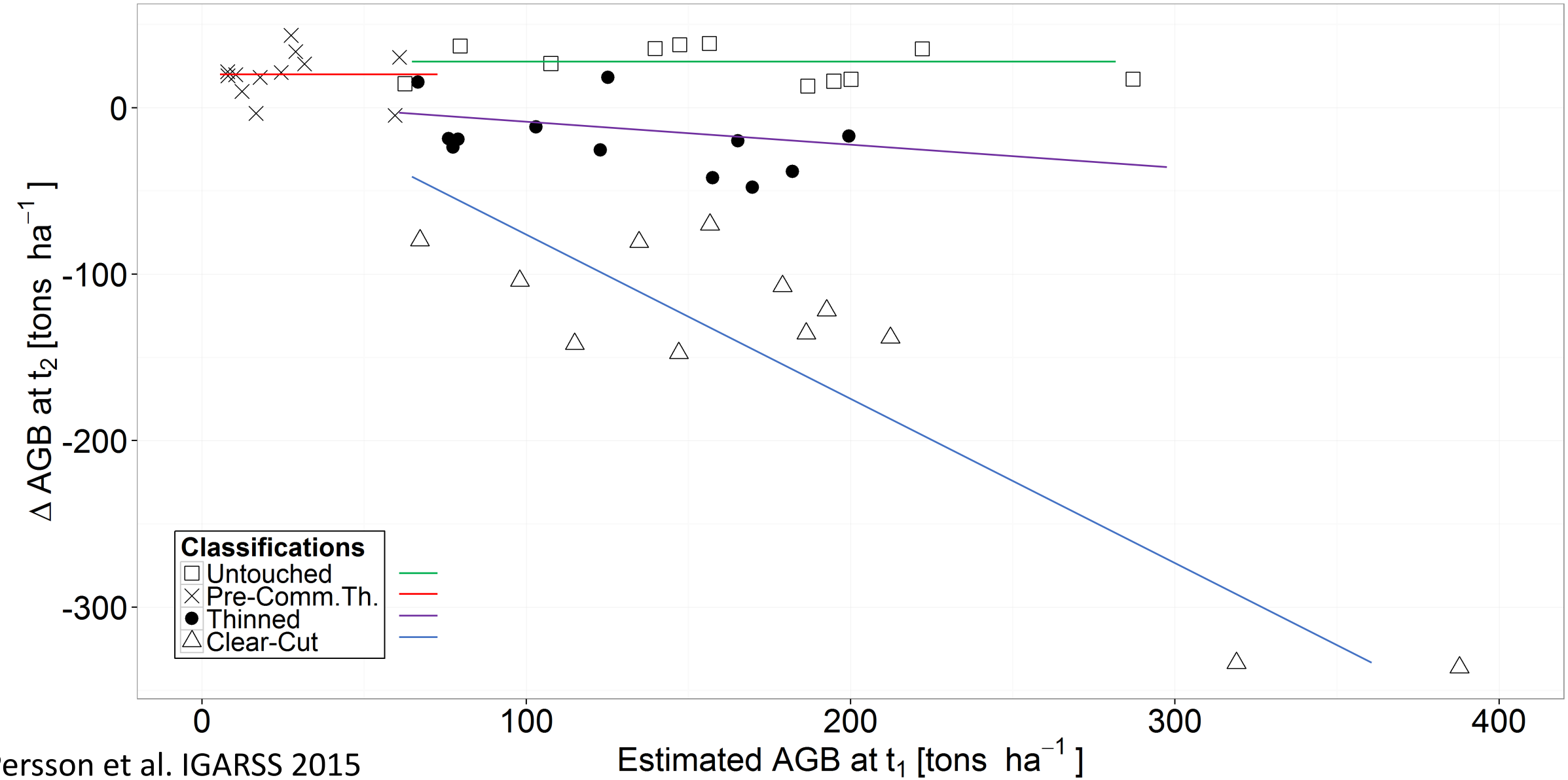

Persson et al. IGARSS 2015

Use of Polarization

- Linear (HH, HV, VH, VV), circular or elliptical polarizations
- Sending vs. receiving polarization

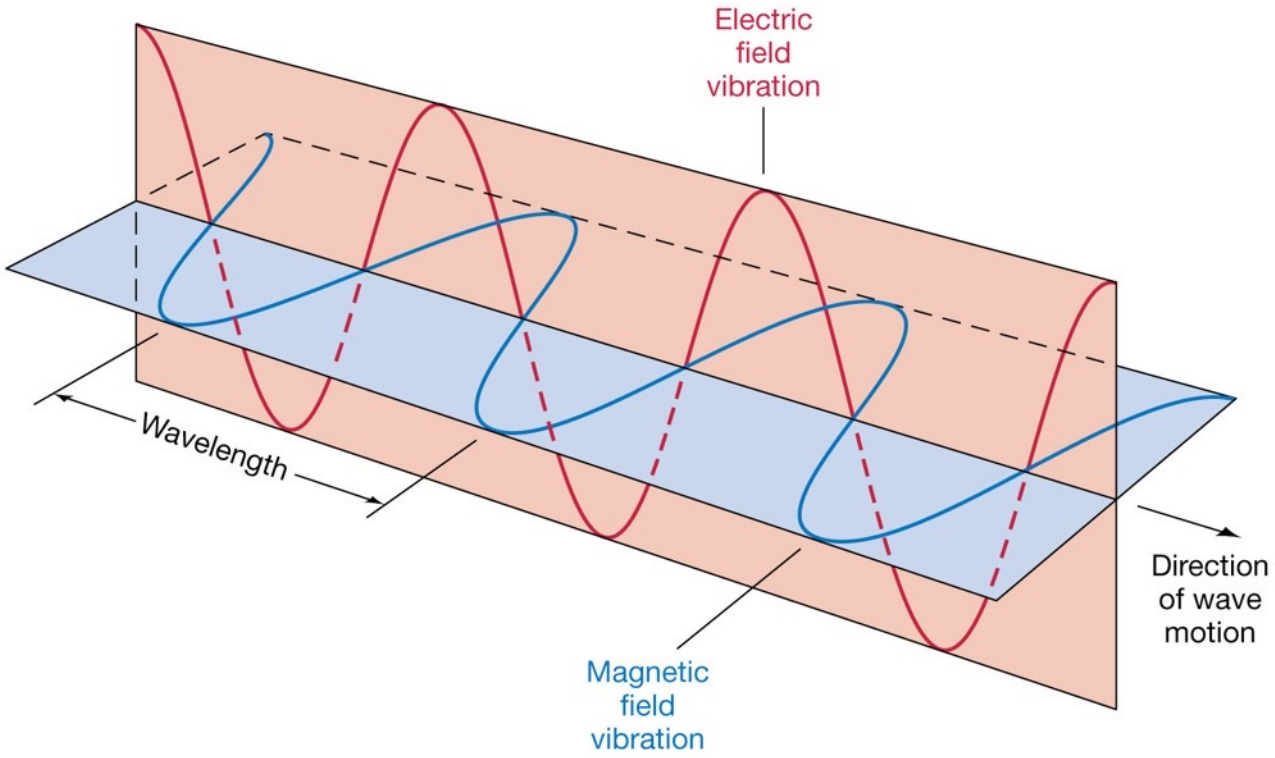

Penetration of vegetation

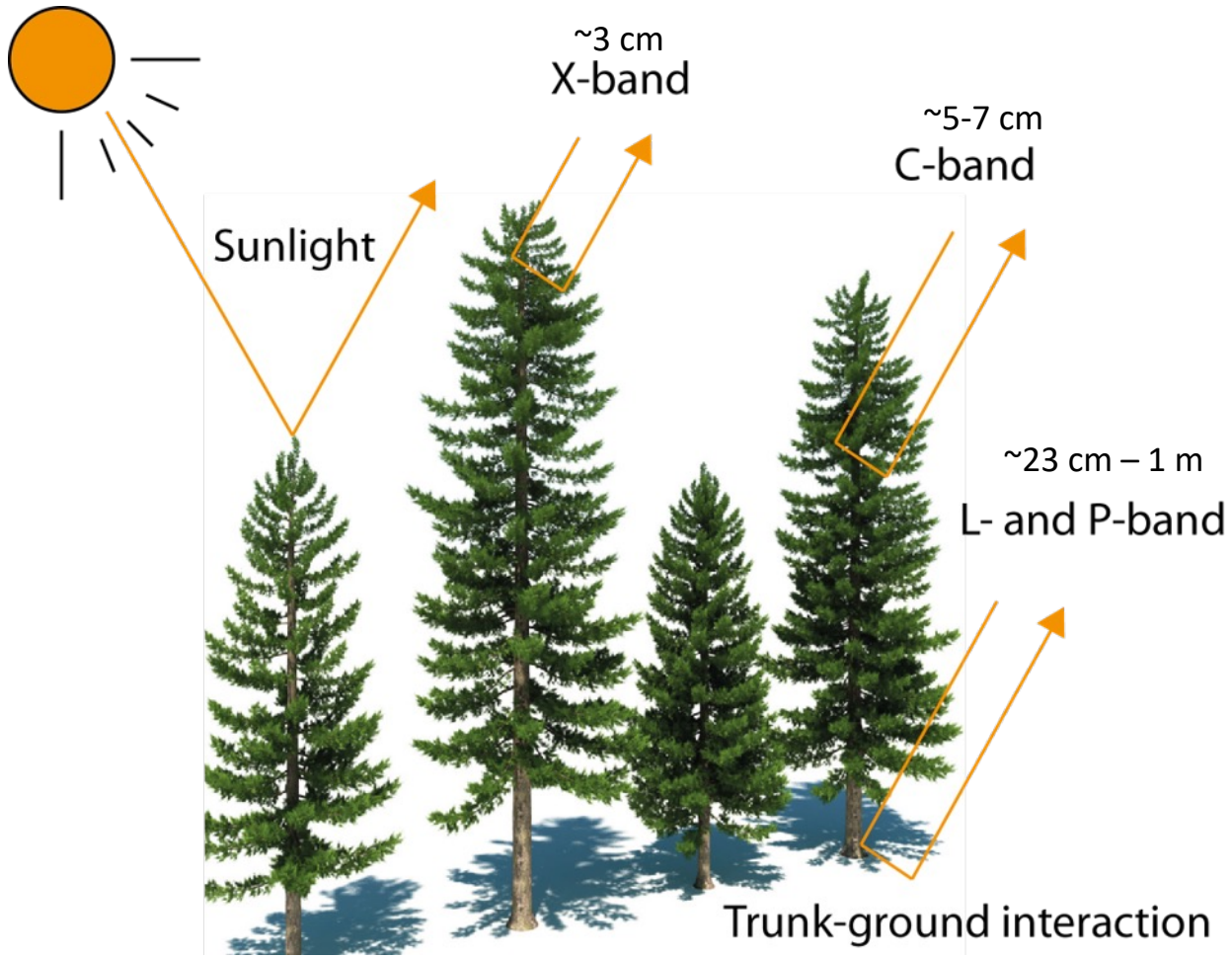

Radar bands

Band name	Frequency range	Wavelength range	Description
VHF	30-300 MHz	1-10 m	Very High Frequency
P	250-500 MHz	0.6-1.2 m	P for "previous"
L	1-2 GHz	15-30 cm	L for “long” wave
S	2-4 GHz	7.5-15 cm	S for “short” wave
C	4-8 GHz	3.75-7.5 cm	C for “compromise”
X	8-12 GHz	2.5-3.75 cm	X for crosshair
Ku	12-18 GHz	1.7-2.5 cm	Ku for “kurz-unten”
K	18-27 GHz	1.1-1.7 cm	German “kurz” (short)
Ka	27-40 GHz	0.75-1.1 cm	Ka for “kurz-above”

Backscatter vs. AGB saturates for shorter wavelengths

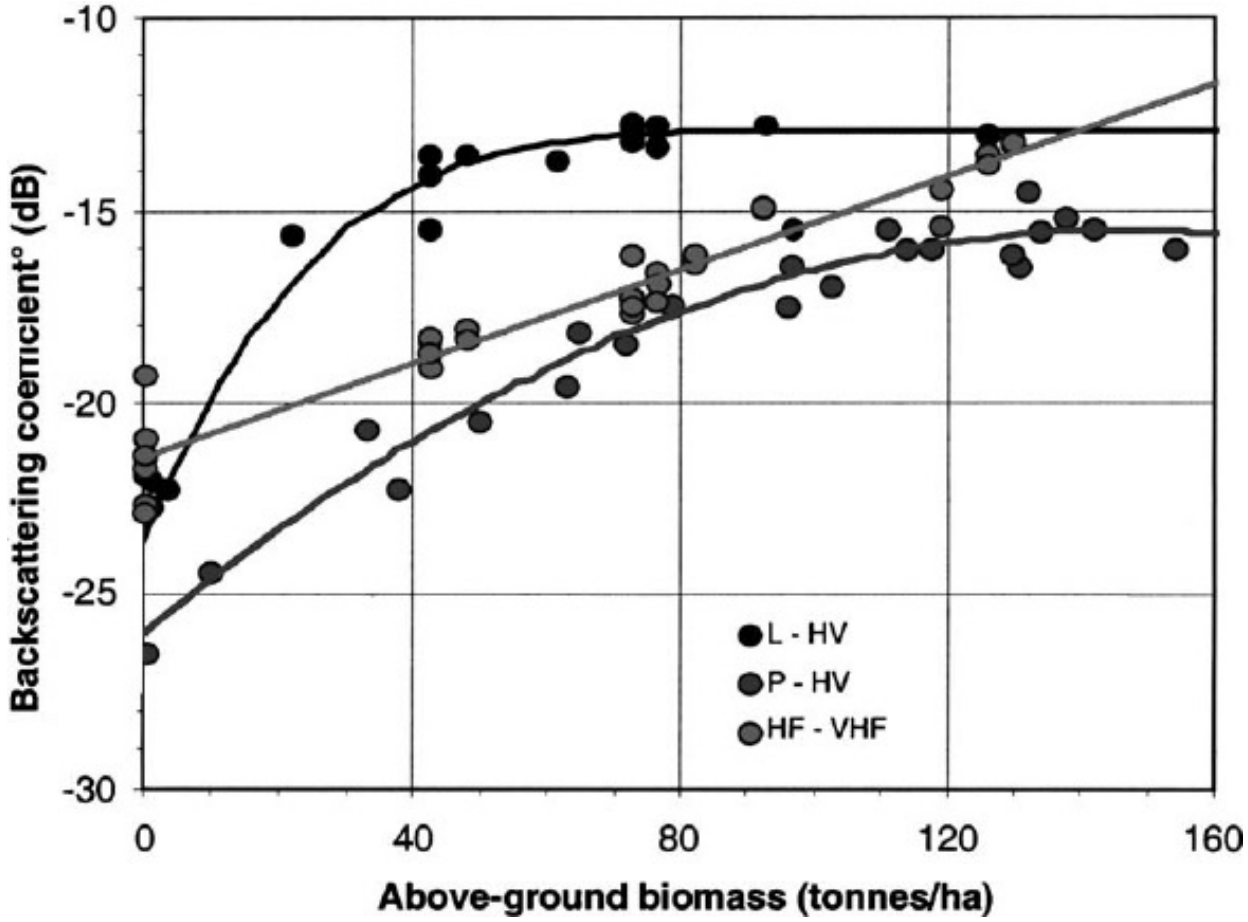

Note: This graph shows the saturation of SAR backscatter from the L-band (dark top line), P-band (gray bottom), and VHF-band (light gray, middle) over a forest in Landes, France. In this study, L- and P-band sensitivity to increasing biomass is limited after 100 tons/ha; other studies have achieved higher sensitivity by combining polarizations.
Source: Le Toan et al. 2004

Polarimetry – decomposing SAR signal

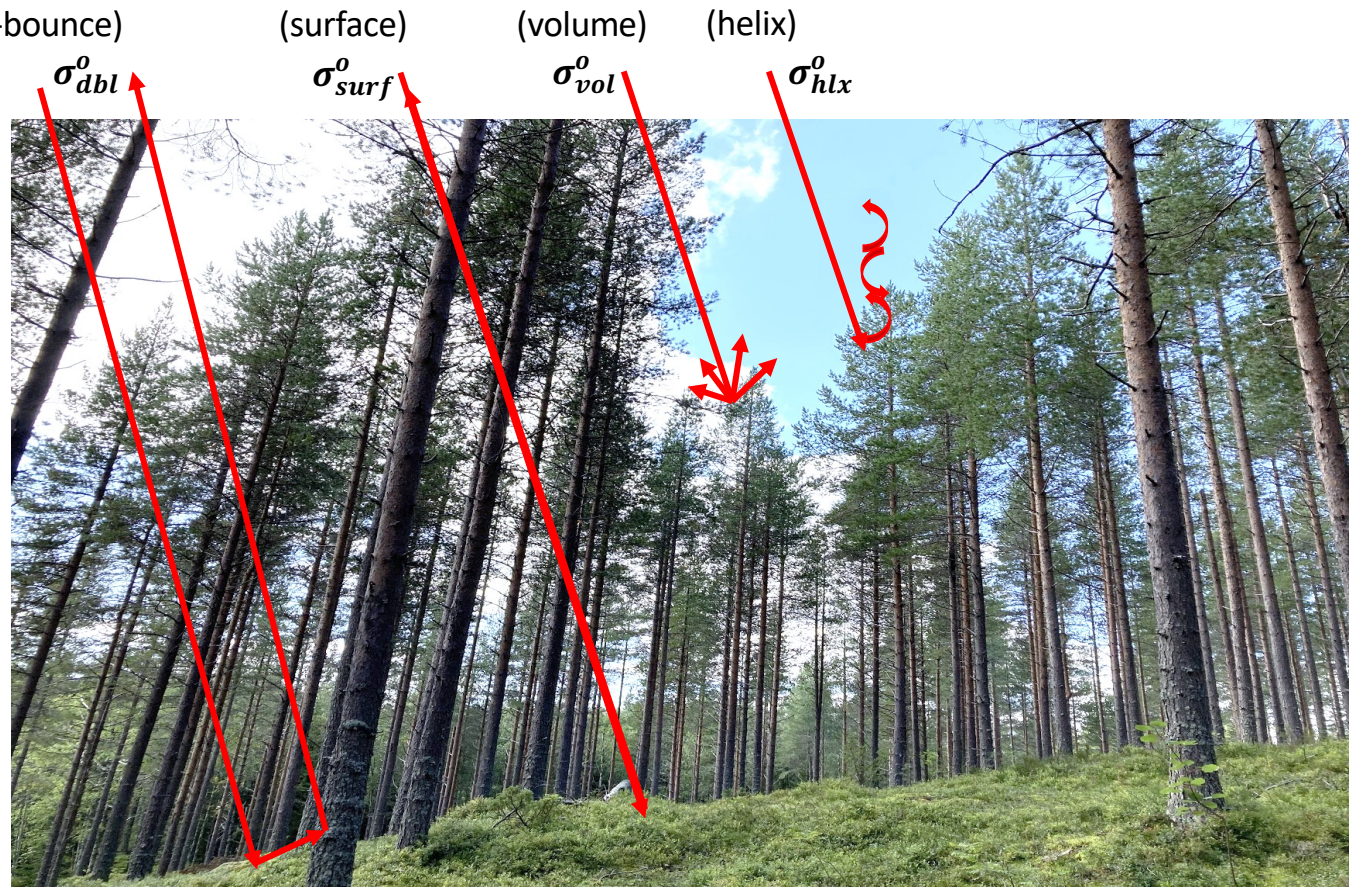

Applied Yamaguchi Four-component Decompositions in linear regression model:

$$\mathrm{AGB} = a + b\sigma^o_{dbl} + c\sigma^o_{vol} + d\sigma^o_{surf} + f\sigma^o_{hlx} + \varepsilon$$

AGB estimated from polarimetric SAR

RadarSat-2 (C-band)

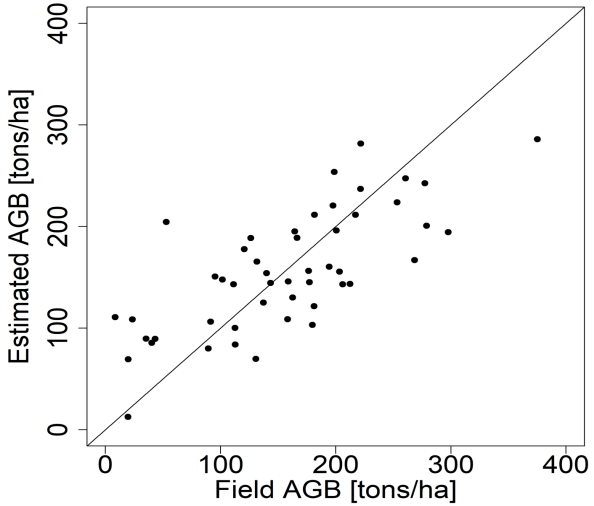

TerraSAR-X (X-band)

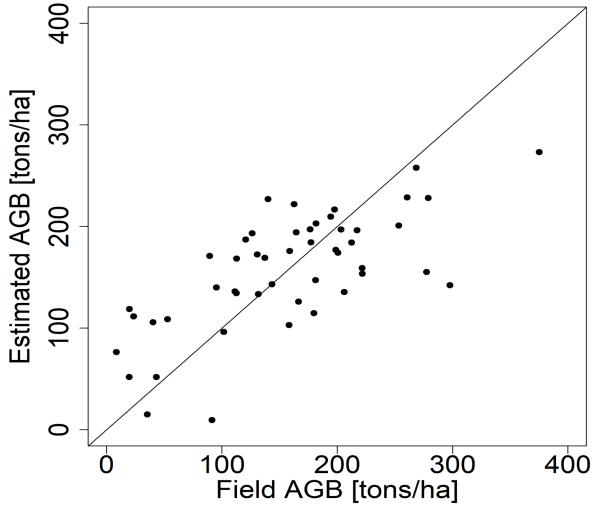

Sensor	Model	R^2_{adj}	RMSE [tons/ha]	n
RadarSat-2	Estimated	0.52	54.2 (34.6%)	48
TerraSAR-X	Estimated	0.47	56.8 (36.3%)	48
RadarSat-2	LOOCV	-	58.1 (37.1%)	48
TerraSAR-X	LOOCV	-	60.6 (38.6%)	48

Mapping tree species using SAR

remote sensing 2021

Article

Assessing Forest Type and Tree Species Classification Using Sentinel-1 C-Band SAR Data in Southern Sweden

Alberto Udali [1,*], Emanuele Lingua [1] and Henrik J. Persson [2]

- OA=0.94 for two forest types
- OA=0.66 for four tree species

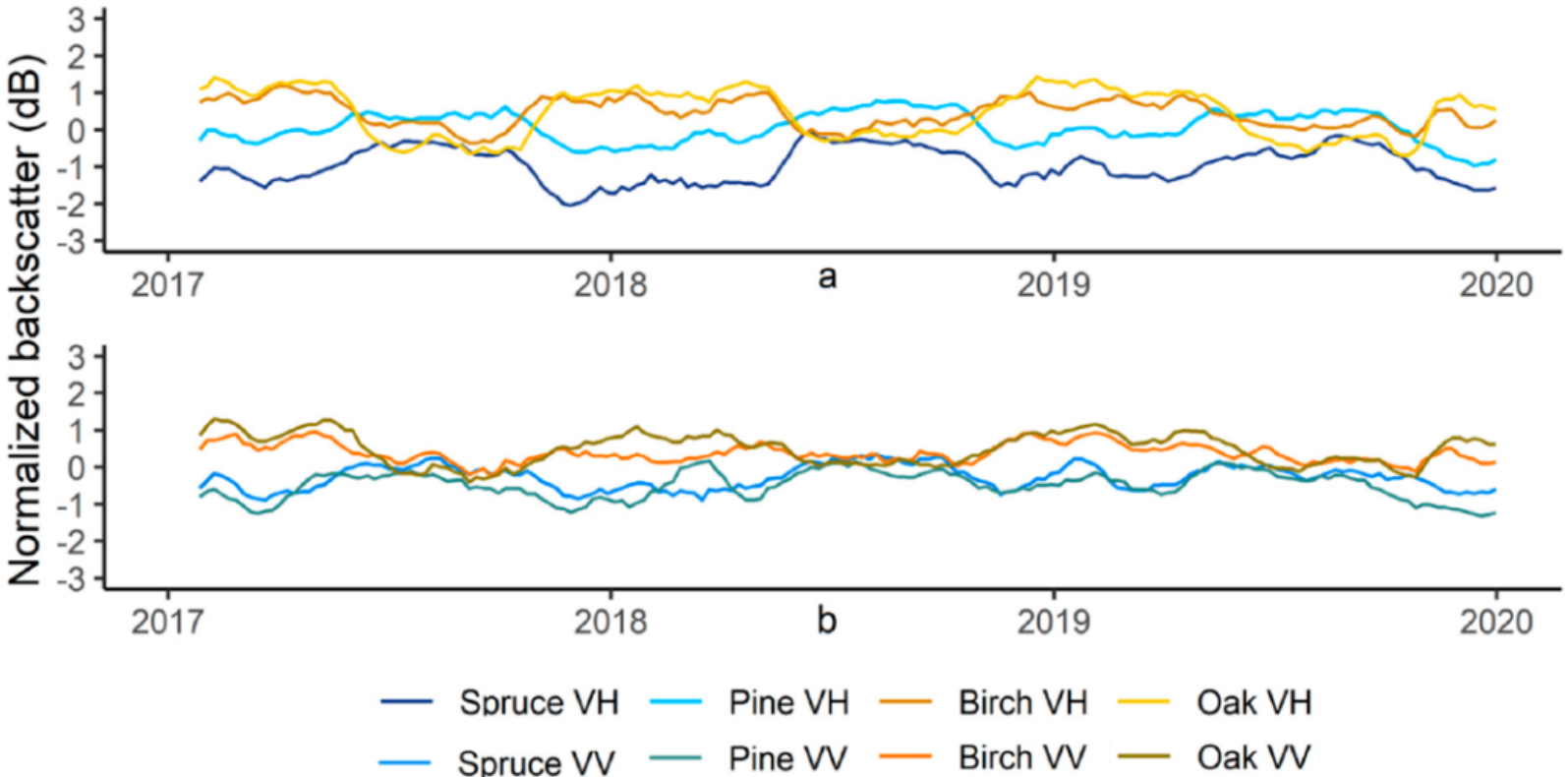

International Journal of Applied Earth Observations and Geoinformation 96 (2021) 102275

Contents lists available at ScienceDirect

International Journal of Applied Earth Observations and Geoinformation

journal homepage: www.elsevier.com/locate/jag

Combining TanDEM-X and Sentinel-2 for large-area species-wise prediction of forest biomass and volume

Henrik J. Persson *, Jonas Jonzén, Mats Nilsson

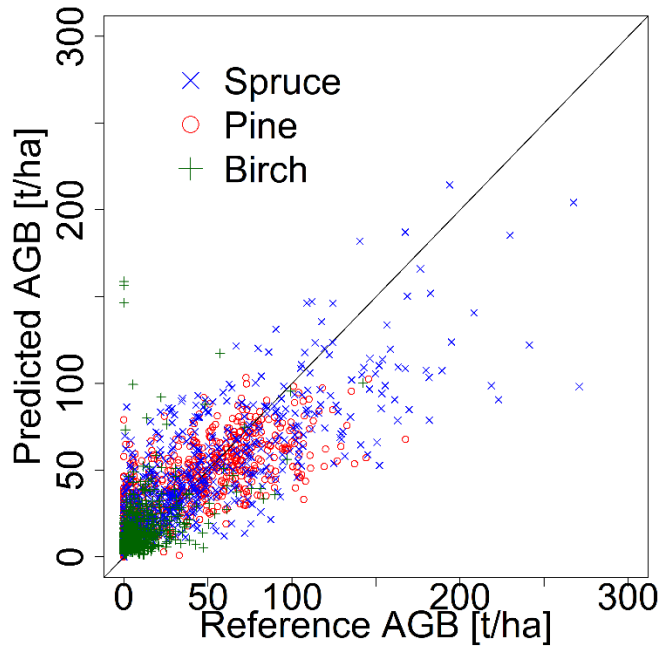

- kNN method – k=5 neighbors
- Spectral data Sentinel-2 and height from TanDEM-X
- OA=0.77 for majority tree species – three tree species

Forest parameter estimation

Results and conclusions

- Biomass was estimated accurately using TanDEM-X InSAR
- Biomass change could be estimated successfully for 3 different actions
- Biomass was estimated relatively accurately using quad-pol Radarsat-2 and TerraSAR-X
- Biomass was not estimated sufficiently accurate using dual-pol Radarsat-2
- Biomass change was not possible to estimate using dual-pol Radarsat-2
- SAR can be used to map tree species, but short wavelengths provide better information about volume than tree species

Forest parameter estimation

Further research plan

- Analyze impact of weather on radar measurements
  – Developing correction algorithms by including e.g., precipitation and temperature data at a tower experiment.
  – Upscale methods to satellite based SAR images.

- Detection and mapping of storm damaged forest using spaceborne synthetic aperture SAR
  –Developing methodology and algorithms
  –Perform a scientific evaluation of SAR data from satellite sensors for detecting and mapping changes in boreal forests.

- Exploring the method of tree crown extraction by combining satellite image and LiDAR data for multi-scale regional biomass dynamic monitoring with Sentinel-1 SAR data.

Three years of collaborative research

- Co-supervising one visiting PhD student from BFU to SLU from 2022 to 2023.
- Joint research on the early detection of pine wilt disease using hyperspectral data, publishing one research paper, two conference papers, and one manuscript under review.
- Research seminars and discussions.
- Teaching in doctoral courses.

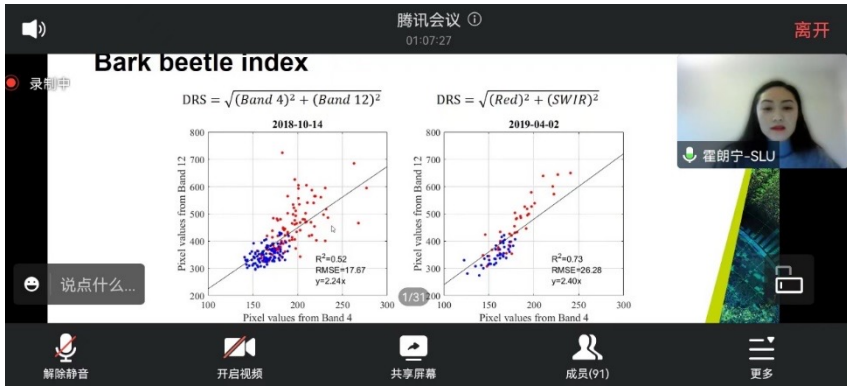

Papers

- Chen L, Wu J, Xie Y, et al. Discriminative feature constraints via supervised contrastive learning for few-shot forest tree species classification using airborne hyperspectral images[J]. ***Remote Sensing of Environment***, 2023, 295: 113710.
- Chen L, Wei Y, Yao Z, et al. Data augmentation in prototypical networks for forest tree species classification using airborne hyperspectral images[J]. ***IEEE Transactions on Geoscience and Remote Sensing***, 2022, 60: 1-16.
- Li Y, Chai G, Wang Y, et al. Ace r-cnn: An attention complementary and edge detection-based instance segmentation algorithm for individual tree species identification using uav rgb images and lidar data[J]. ***Remote Sensing***, 2022, 14(13): 3035.
- Chen L, Tian X, et al. A New CBAM-P-Net Model for Few-Shot Forest Species Classification Using Airborne Hyperspectral Images[J]. ***Remote Sensing***, 2021, 13, 1269. 未标注
- Wang Y, Jia X, Chai G, et al. Improved estimation of aboveground biomass of regional coniferous forests integrating UAV-LiDAR strip data, Sentinel-1 and Sentinel-2 imageries[J]. ***Plant Methods***, 2023, 19(1): 1-19.
- Chai G, Zheng Y, Lei L, et al. A novel solution for extracting individual tree crown parameters in high-density plantation considering inter-tree growth competition using terrestrial close-range scanning and photogrammetry technology[J]. ***Computers and Electronics in Agriculture***, 2023, 209: 107849.
- Lei L, Yin T, Chai G, et al. A novel algorithm of individual tree crowns segmentation considering three-dimensional canopy attributes using UAV oblique photos[J]. ***International Journal of Applied Earth Observation and Geoinformation***, 2022, 112: 102893.
- Lei L, Chai G, Wang Y, Jia X, Yin T, Zhang X. Estimating Individual Tree Above-Ground Biomass of Chinese Fir Plantation: Exploring the Combination of Multi-Dimensional Features from UAV Oblique Photos[J]. ***Remote Sensing***. 2022, 14(3):504.
- Wang Y, Zhang X, Guo Z. Estimation of tree height and aboveground biomass of coniferous forests in North China using stereo ZY-3, multispectral Sentinel-2, and DEM data[J]. ***Ecological Indicators***, 2021, 126, 107645.
- Li H, Chen L, Yao Z, Li N, Long L, Zhang X. Intelligent Identification of Pine Wilt Disease Infected Individual Trees Using UAV-Based Hyperspectral Imagery. ***Remote Sensing***, 2023; 15(13):3295.
- Long L, Chen Y, Song S, et al. Remote Sensing Monitoring of Pine Wilt Disease Based on Time-Series Remote Sensing Index[J]. ***Remote Sensing***, 2023, 15(2): 360.
- Li N, Huo L, Zhang X. Classification of pine wilt disease at different infection stages by diagnostic hyperspectral bands[J]. ***Ecological Indicators***, 2022, 142: 109198.
- Li N, Zhang X, Huo L. Identifying Nematode-Induced Wilt Using Hyperspectral Drone Images and Assessing the Potential of Early Detection[C]//***IGARSS 2022-2022 IEEE International Geoscience and Remote Sensing Symposium***. IEEE, 2022: 512-515.

Papers

- Huo, L., Persson, H.J., Bohlin, J., & Lindberg, E. (2023). Green-attack detection or Overfitting? Comparing Machine-learning- and Vegetation-index-based Methods to Early Detect European Spruce Bark Beetle Attacks Using Multispectral Drone Images. In IGARSS 2023 IEEE International Geoscience and Remote Sensing Symposium.
- Huo, L., Lindberg, E., Bohlin, J., & Persson, H.J. (2023). Assessing the detectability of European spruce bark beetle green attack in multispectral drone images with high spatial- and temporal resolutions. Remote Sensing of Environment, 287, 113484.
- Huo, L., Lindberg, E., Fransson, J.E.S., & Persson, H.J. (2022). Comparing Spectral Differences Between Healthy and Early Infested Spruce Forests Caused by Bark Beetle Attacks using Satellite Images. In IGARSS 2022 IEEE International Geoscience and Remote Sensing Symposium (pp. 7709–7712): IEEE.
- Huo, L., Persson, H., Lindberg, E., (2021). Early detection of forest stress from European spruce bark beetle attack, and a new vegetation index: Normalized Distance Red & SWIR (NDRS). Remote Sensing of Environment, 255, 112240.
- Huo, L., Lindberg, E., & Persson, H. (2020). Normalized Projected Red & SWIR (NPRS): A New Vegetation Index for Forest Health Estimation and Its Application on Spruce Bark Beetle Attack Detection. In IGARSS 2020 IEEE International Geoscience and Remote Sensing Symposium (pp. 4618–4621): IEEE.
- Persson, H., Huo, L., Lindberg, E., & (manuscript). Using the distance red swir index – DRS –with Sentinel-2 satellite images for operational large-area bark beetle mapping
- Huo, L., Lindberg, E., & Persson, H. (Under reveiw). Analyzing the Environmental Risk Factors of European Spruce Bark Beetle Damage At the Local Scale
- Huuva, I., Persson, H.J., Wallerman, J., Fransson, J.E.S. 2022. Detectability of forest management actions in time series of penetration depth corrected TanDEM-X phase heights. IGARSS 2022, Kuala Lumpur, Malaysia.
- Huuva, I., Wallerman, J., Fransson, J.E.S., Persson, H.J., 2023. Prediction of Site Index and Age Using Time Series of TanDEM-X Phase Heights. Remote Sens. 15, 1–16.
- Persson, H.J., Fransson, J.E.S., 2017. Comparison between TanDEM-X and ALS based estimation of above ground biomass and tree height in boreal forests. Scand. J. For. Res. 32, 306–319. https://doi.org/10.1080/02827581.2016.1220618
- Persson, H.J., Fransson, J.E.S., 2016. Estimating Site Index From Short-Term TanDEM-X Canopy Height Models. IEEE J. Sel. Top. Appl. Earth Obs. Remote Sens. 9, 3598–3606. https://doi.org/10.1109/JSTARS.2016.2563158
- Persson, H.J., Jonzén, J., Nilsson, M., 2021. Combining TanDEM-X and Sentinel-2 for large-area species-wise prediction of forest biomass and volume. Int. J. Appl. Earth Obs. Geoinf. 96, 10. https://doi.org/10.1016/j.jag.2020.102275
- Persson, H.J., Olsson, H., Soja, M.J., Ulander, L.M.H., Fransson, J.E.S., 2017. Experiences from large-scale forest mapping of Sweden using TanDEM-X data. Remote Sens. 9, 1253–1279. https://doi.org/10.3390/rs9121253
- Persson, H.J., Axelsson, C., Mukhopadhay, R., Holmgren, J. 2023. Comparison of single tree species classification using very dense ALS data or dual-wave ALS data. IGARSS 2023, Pasadena, USA.
- Persson, H.J., Soja, M.J. 2015. Detection of thinning and clear-cuts using TanDEM-X data. IGARSS 2015 Symposium, Remote Sensing for a Dynamic Earth, Milan, Italy.
- Udali, A., Lingua, E., Persson, H.J., 2021. Assessing Forest Type and Tree Species Classification Using Sentinel-1 C-Band SAR Data in Southern Sweden. Remote Sens. 13.

Thank You!

Beijing Forestry University

PI China: Prof. Xiaoli Zhang
Chinese investigators:
Dr. Ning Zhang
Dr. Yueting Wang
Dr. Niwen Li
Dr. Guoqi Chai
Dr. Lingting Lei
Dr. Long Chen
Dr. Xiang Jia
Dr. Zongqi Yao

Swedish University of Agricultural Sciences

PI Europe: Dr. Langning Huo
European investigators:
Dr. Langning Huo
Dr. Henrik Persson
Dr. Eva Lindberg
Dr. Ivan Huuva

EO Data Delivery

The satellite images acquired for the study areas in China are:

- Sentinel-1, time-series images from 2019 to 2022, covering Gaofeng and Wangyedian.
- Sentinel-2, time-series cloud-free images from 2019 to 2022, covering Gaofeng, Lu'an, Wangyedian, Genhe, and Pu'er.
- Gaofen-1/2/6, 315 images from 2021 to 2022, covering Gaofen, Genhe and Pu’er.
- Radarsat-2, one image covering Fushun and one image covering Qingyuan.

The satellite images acquired in Remningstorp, Sweden are:

- Sentinel-2, time-series cloud-free images from 2018 to 2021.
- WorldView-3, one SWIR image (June 2021).
- Radarsat-2, one image each in 2020 and 2021.
- Pleiades, one image (29 Apr 2021).